Scientific report; WR 94-05

*Ministerie van Verkeer en Waterstaat*

Koninklijk Nederlands
Meteorologisch Instituut

# Spectral Ultraviolet Radiation Measurements and Correlation with Atmospheric Parameters

*F. Kuik*
*H. Kelder*

De Bilt, 1994

KNMI

Scientific report; WR 94-05

De Bilt, 1994

Postbus 201
3730 AE De Bilt
Wilhelminalaan 10
Telefoon 030-206 911
Telefax 030-210 407

UDC: 551.509.329
551.510.534
551.521.17
ISBN: 90-369-2065-5
ISSN: 0169-1651

# Spectral Ultraviolet Radiation Measurements and Correlation with Atmospheric Parameters

Final report NOP project 852088

F. Kuik, H. Kelder

*KNMI, P.O. Box 201, 3730 AE De Bilt, The Netherlands*

November 15, 1994

# Contents

# Chapter 1

# Ultraviolet Radiation in the Earth Atmosphere

## 1.1 Introduction

This report describes the UV-research that has been done at the KNMI since 1991, when NOP project no. 852088 started. The project leader was Dr. H. Kelder, and the first activities were carried out by Drs. W. Slob, who retired in October 1992. In November 1992 Dr. F. Kuik was employed to continue the UV-activities at the KNMI. Other persons at the KNMI involved in this NOP project are Drs. R. van Dorland (radiation modelling), Dr. A. van Lammeren (radiation measurements), and C. Hofman (technical assistance). Dr. P. Stammes and Dr. W. Wauben, although not mentioned in the NOP-contract, were closely involved in the spectral UV-radiative transfer calculations.

When Slob started UV-research at the KNMI spectral UV-measurements were still considered as very sophisticated. His philosophy was that this would remain the case, even with the development of new instruments. Therefore, he made the choice to start two types of UV-measurements: spectral UV-measurements and narrow band UV-measurements.

Spectral UV-measurements are necessary to study correlations with ozone. Absorption features in the Hartley-Huggins absorptions bands are approximately 2 nm wide. To study the correlation between ozone and UV, spectral measurements should be performed at least every 0.5 nm. In medical and biological sciences various action spectra are frequently used to describe effects of UV-radiation on different systems. This can also only be done if spectral UV-measurements are available. However, for monitoring purposes it is more convenient to have additional 'simple' instruments that require little maintenance, are (relatively) cheap, and easy to handle in the sense that they do not require highly educated operators. A well known broad band instrument that fulfills these requirements is the Robertson-Berger meter. A disadvantage of this instrument, however, is that it measures the integrated amount of UV-radiation between 280 and 400 nm, and that it produces a 'sunburn' equivalent reading. Any information on the spectral characteristics of the UV will therefore be lost. This means that it can only be used for UV-monitoring in a relative way (it does not produce UV-irradiances in $Wm^{-2}$), and processes that have other spectral sensitivity characteristics than the fixed instrument's spectral response cannot be studied. Slob (and later Kuik) developed in cooperation with Kipp & Zonen (Delft) two narrow band UV-instruments, one in the UVA and one in the UVB wavelength region. If the bandwidth are chosen in a sensible way, there will be a good correlation with spectral UV-measurements. These narrow band

instruments (they are discussed in Chap. 2) are currently in use at the KNMI as monitoring devices.

In this chapter UV-radiation and its relation with ozone and other atmospheric parameters are discussed. We start with some definitions and basic concepts on ultraviolet radiation and ozone. Results of our spectral UV-radiative transfer calculations, and measurements are shown throughout this report. The radiative transfer calculations, UV-measurements, instruments, and calibration procedures will be discussed separately in later chapters.

## 1.2 Ultraviolet Radiation

Ultraviolet radiation (UV) is usually defined as electromagnetic radiation with wavelengths between 100 and 400 nm. In the electromagnetic spectrum UV is bounded at the short wavelength side by X-rays and $\gamma$-radiation, and at the long wavelength side by visible radiation. Short wavelength radiation has a high energy contents per photon, and it is harmful or even dangerous for many living organisms. UV-radiation can be subdivided into three regions according to the wavelength.

**UVC** Radiation in the wavelength region 100-280 nm. It is the most energetic UV-radiation. DNA is extremely sensitive to UVC, but since all UVC is absorbed by oxygen and ozone, it does not pose an environmental problem.

**UVB** Radiation between 280 and 315 nm; the upper limit of 315 nm is according to WMO (World Meteorological Organization) standards (see, for example, Guide to Meteorological Instruments and Methods of Observations, Chap. 9, pp. 9.2), but 320 nm is also frequently used. UVB is partly absorbed by ozone and as a result only radiation with wavelengths larger than approximately 290 nm is observed at sea level. All living organisms are sensitive to UVB radiation. In combination with ozone depletion UVB can become an environmental hazard.

**UVA** UVA is much less energetic than UVC and UVB. However, almost all the solar UVA is transmitted through the atmosphere, since it is hardly absorbed by ozone or any other atmospheric constituents. Human skin is very sensitive to UVB, and to a lesser extend to UVA. However, there is much more UVA in solar radiation than UVB. Therefore, UVA can still contribute to some types of skin cancer (Van der Leun 1994). It thus is a misconception that UVA is a harmless type of UV-radiation.

In Fig. 1.1 a typical measured UV spectrum for a clear summer day in De Bilt is shown, together with the extraterrestrial solar spectrum (Vanhoosier *et al.* 1988). Note the sharp cut-off below 310 nm due to absorption of UVB-radiation by ozone. Approximately 8.5% of the solar energy that is incident at the top of our atmosphere is in the UV-part of the spectrum. UVC accounts for 0.5%, UVB and UVA for 1.4% and 6.5%, respectively. In Table 1.1 the energy distribution of the extraterrestrial solar radiation is given based on a solar constant of 1367.2 $Wm^{-2}$ (Frederick *et al.* 1989).

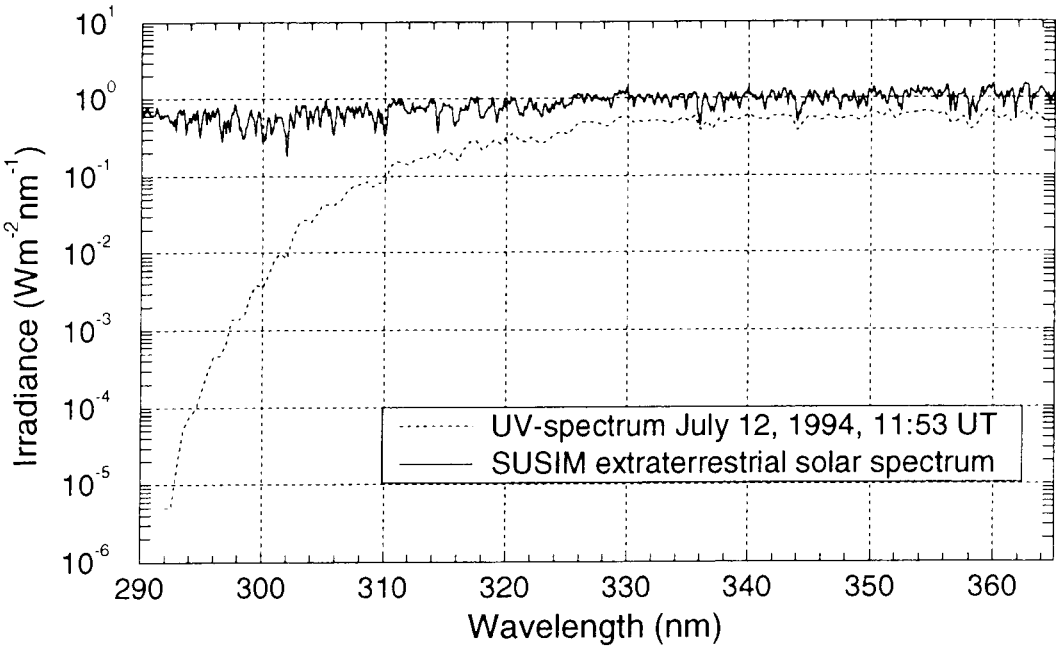


**Figure 1.1** The extraterrestrial solar spectrum, and the UV-spectrum measured in De Bilt on July 12, 1994, with Brewer #100. The measurement was performed at 11:53 UT for a solar elevation of 59.8°.

Ultraviolet radiation measured at sea level spans a wavelength region from 290 to 400 nm. This makes it difficult to discuss 'the amount of UV-radiation' inferred from spectral measurements or calculations, because a spectrum contains about 220 numbers (measurements at 0.5 nm increment) representing UV-irradiances at certain wavelengths. Therefore the dose rate $\mathrm{d}D/\mathrm{d}t$ ($\mathrm{mWm}^{-2}$) is introduced as the weighed wavelength integrated UV by (cf. Dahlback *et al.* 1989)

$$\frac{\mathrm{d}D}{\mathrm{d}t} = \int_{100}^{400} I(\lambda)A(\lambda)\,\mathrm{d}\lambda, \tag{1.1}$$

**Table 1.1** Energy distribution of the extraterrestrial solar energy at the top of our atmosphere based on a solar constant of 1367.2 $\mathrm{Wm}^{-2}$ (Frederick *et al.* 1989).

| Spectral region | Irradiance ($\mathrm{Wm}^{-2}$) | % of total energy |
|---|---|---|
| UVC ($\lambda < 280$ nm) | 6.4 | 0.5 |
| UVB ($280 \leq \lambda < 315$ nm) | 18.5 | 1.4 |
| UVA ($315 \leq \lambda < 400$ nm) | 88.3 | 6.5 |
| Visible ($400 \leq \lambda < 700$ nm) | 532.0 | 38.9 |
| Infrared ($\lambda \geq 700$ nm) | 722.0 | 52.8 |

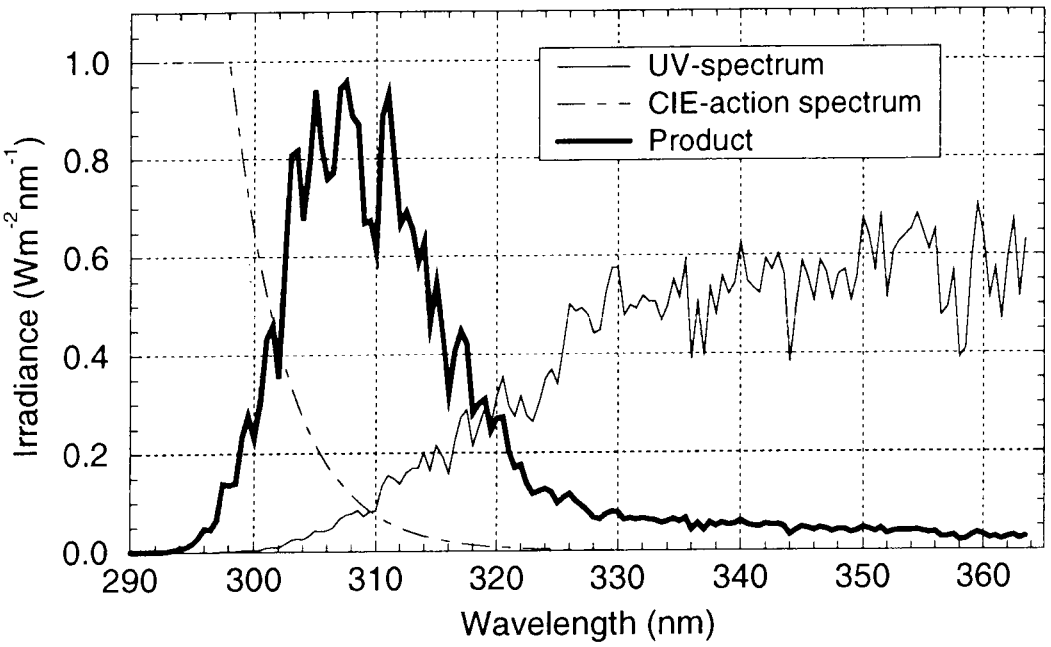


**Figure 1.2** The CIE-action spectrum $A(\lambda)$ from Eq.(1.2), a measured UV-spectrum, and the product of the two (the product spectrum was divided by 10 to fit the scale of the graph). It is clear from the figure that the weighed spectrum is the most sensitive to UVB-radiation, and only for a small part to UVA.

where $\lambda$ is the wavelength in nm, $I(\lambda)$ is the spectral UV-irradiance in mWm$^{-2}$nm$^{-1}$. $A(\lambda)$ is an action spectrum describing the wavelength dependent sensitivity of a certain process (or organism) to UV-radiation. Although the integration is over the entire UV-wavelength region, in practice the lower integration boundary will be 290 nm. In this report $A(\lambda)$ is the CIE-action spectrum (also called McKinlay-Diffey action spectrum, cf. McKinlay and Diffey 1987) defined by

$$\begin{aligned} A(\lambda) &= 1.0 && \lambda \leq 298 \text{ nm} \\ A(\lambda) &= 10^{0.094(298-\lambda)} && 298 < \lambda \leq 328 \text{ nm} \\ A(\lambda) &= 10^{0.015(139-\lambda)} && 328 < \lambda \leq 400 \text{ nm}. \end{aligned} \tag{1.2}$$

This action spectrum is a mathematical representation of the sensitivity of 'the human skin' for sunburn. The action spectrum and the effect of weighing the spectral UV-radiation are shown in Fig. 1.2. The total dose, $D$, is obtained by integrating Eq.(1.1) over the time the exposure takes place. From hereon the dose rate will be called Damaging UV (DUV).

Although the CIE-action spectrum is a sunburn action spectrum, it is also frequently used to represent amounts of UV for other processes in which UVB is a dominant factor. In this report DUV will also be used to present amounts of UV-radiation by a single number. Other commonly used action spectra are a generalized DNA damage spectrum (Setlow 1974), and a generalized plant damage spectrum (Caldwell *et al.* 1986). They will not be used nor discussed any further in this report.

## 1.3 Effects of Ozone on Ultraviolet Radiation

Ozone is a trace gas in the atmosphere that absorbs UV-radiation in a very efficient manner. In doing so, it protects all life forms on Earth from damaging UVB-radiation. Approximately 90% of all ozone in the atmosphere is found in the stratosphere, and only 10% in the troposphere. It is a reactive gas, of which the molecules consist of three oxygen atoms. It is constantly created and destroyed under the influence of UV-radiation in the stratosphere.

In Whitten and Prasad (1985, Chap. 2), Wayne (1991), and many other textbooks on atmospheric chemistry, ozone chemistry is treated in detail. Some of the basic reactions will be briefly discussed here. Molecular oxygen is dissociated by UVC-radiation in the Schumann-Runge bands between 170 and 195 nm, and in the Herzberg bands and continuum between 195 and 260 nm. the products are two ground state oxygen atoms

$$O_2 + h\nu \rightarrow 2O. \tag{1.3}$$

The atoms associate rapidly with the abundantly available oxygen molecules, creation an ozone molecule by

$$O_2 + O + M \rightarrow O_3 + M. \tag{1.4}$$

M is a mass that is needed to remove energy that is released during the creation of the ozone molecule. This is the most important stratospheric ozone production process, mainly taking place at altitudes above 30 km.

Ozone molecules can absorb UVB and UVC-radiation, as can be seen from Fig. 1.3. In the process the molecule breaks up in molecular oxygen plus an oxygen atom,

$$O_3 + h\nu \rightarrow O_2 + O. \tag{1.5}$$

This production/destruction scheme of ozone was first suggested by Chapman (1930). Due to variations in the atmospheric density as a function of altitude, an equilibrium in ozone concentration will establish, which is also altitude dependent. The maximum ozone concentration is found roughly between 10 and 40 km altitude and is commonly called 'the ozone layer'.

Although Chapman's scheme still describes the basic stratospheric ozone cycle, it is known not to represent the observed ozone distribution in a correct manner. For a more accurate description, chemical reactions involving free radicals have to be included. These reactions are schematically described by

$$X + O_3 \rightarrow XO + O_2, \tag{1.6}$$

$$XO + O \rightarrow X + O_2. \tag{1.7}$$

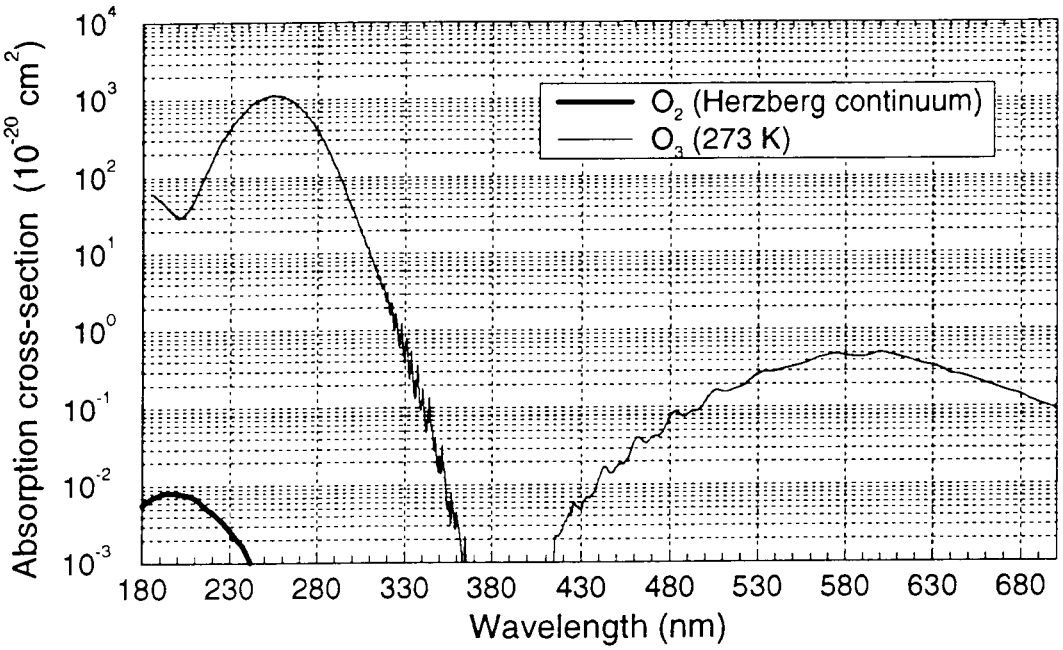


**Figure 1.3** Ozone and molecular oxygen absorption cross-sections per molecule in cm$^2$. The maximum UV-absorption of $O_3$ occurs at 260 nm, while there is hardly any absorption in the UVA between 330 and 405 nm. The strong increase of absorption cross-sections from 330 to 280 nm causes the cut-off in the measured ground level UV-irradiances. The absorption bands for wavelengths larger than 405 nm are called Chapuis bands.

and the net result is

$$O + O_3 \rightarrow 2O_2. \tag{1.8}$$

X is a free radical species, e.g. Cl$^\bullet$, ClO$^\bullet$, Br$^\bullet$, NO$^\bullet$, H$^\bullet$, or OH$^\bullet$. Some of these radicals occur naturally in the stratosphere, some of them are of antropogenic origin. Deviation from a natural chemical equilibrium in the stratosphere, e.g. caused by antropogenic emission of CFCs, can cause depletion of stratospheric ozone.

The total amount of ozone in the vertical direction is usually expressed in Dobson Units, or DU. A 'normal' value for The Netherlands in June is about 350 DU. This means that if all the ozone in the vertical direction above us is brought down to STP, the layer has a thickness of 3.5 mm. In Fig. 1.4 the total column ozone measurements for De Bilt are shown for the period January–October 1994. The measurements that were performed in De Bilt with Brewer #100 are denoted by the bullet and diamond (•, ◇), respectively (the meaning of Direct Sun and Zenith Sky measurements will be explained in Chap. 2, where the Brewer photospectrometer is discussed). In Fig. 1.4 the 'normal' for De Bilt is also shown. This normal was obtained by averaging twelve years of TOMS-satellite ozone observations (Allaart 1994a). From this long term average it can be seen that there is a seasonal variation. The maximum is reached in spring (April), and the minimum in autumn (September-October).

The monthly averages of the total column ozone for 1994 are shown in Table 1.2., as

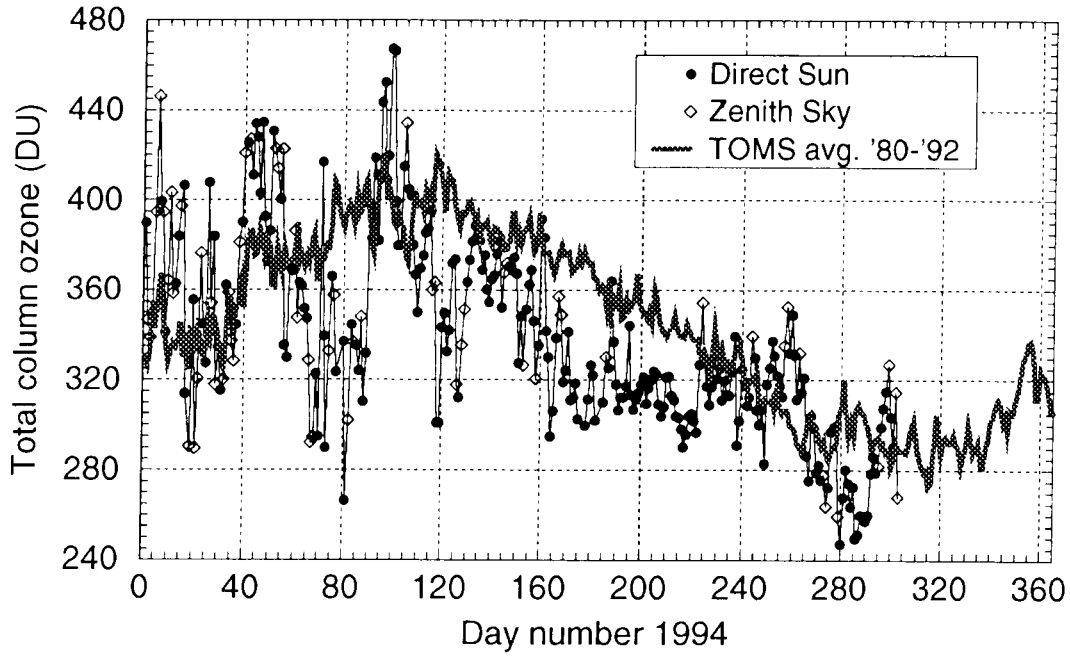


**Figure 1.4** Total column ozone for the period January-October 1994, measured with Brewer #100, at the KNMI in De Bilt.

well as the monthly averages of the normal. From Table 1.2 it can be seen that in 1994 only three months have average ozone values higher than the long term mean. For the first ten months of 1994 the amount of ozone in the atmosphere at De Bilt can be considered to be on the low side. However, seasonal and yearly variations can be considerable, and it is by no means an alarming situation.

Stratospheric ozone depletion may directly result in an increase of UVB-radiation in the biosphere. From model calculations and UV-measurements combined with ozone measurements we found that for clear sky conditions a 1% decrease in ozone results in a 1.3% to 2% increase of the UVB-irradiance (at the short wavelengths) at the Earth surface. The exact number depends on the solar elevation.

The vertical distribution of ozone in the atmosphere also plays an important role. Brühl and Crutzen (1989) stated that increased emissions of $NO_x$ in the industrialized northern hemisphere can lead to an increase of tropospheric ozone, which can overcompensate an increase in UVB-irradiance caused by stratospheric ozone depletion. Tsay and Stamnes (1992) showed that a redistribution of stratospheric ozone to tropospheric ozone tends to decrease surface level UV-irradiances, except for low solar elevations, in which case even an increase of the UV-irradiances can occur when total column ozone decreases. Although the explanations given by Brühl and Crutzen (1989) and Tsay and Stamnes (1992) for similar effects are different, it is clear that ozone depletion and redistribution must both be taken into account in the research of ground level UV-irradiances. At this moment UV-measurements provide contradicting evidence for slightly decreasing and increasing UV-levels (e.g. Scott *et al.* 1988; Kerr and McElroy 1994; Watson *et al.* 1988; Blumthaler and Ambach 1990). The 'long term' spectral UV-measurement series are still very short. It

**Table 1.2** Monthly averages of ozone measurements for De Bilt, January–October 1994, and long term averages from TOMS-satellite measurements. All ozone values are in DU.

| Month | Mean $O_3$ (Brewer) | Minimum | Maximum | TOMS-$O_3$ | % deviation |
|---|---|---|---|---|---|
| January | 360.3 | 289.5 | 407.7 | 339.4 | 6.1 |
| February | 387.6 | 320.0 | 434.4 | 367.4 | 5.5 |
| March | 336.3 | 266.4 | 417.0 | 387.1 | −13.1 |
| April | 391.5 | 300.9 | 467.2 | 398.4 | −1.7 |
| May | 361.6 | 312.4 | 374.7 | 390.8 | −7.5 |
| June | 333.7 | 294.9 | 349.0 | 376.9 | −11.5 |
| July | 318.5 | 302.1 | 363.8 | 352.8 | −9.7 |
| August | 313.5 | 290.2 | 354.3 | 332.5 | −5.7 |
| September | 312.9 | 275.2 | 352.5 | 303.8 | 3.0 |
| October | 278.4 | 242.0 | 268.1 | 295.4 | −5.8 |

will probably not be until some years into the next century before such measurements can provide definite answers on the issue of increasing/decreasing UV-levels.

In Fig. 1.5 the typical daily variation of DUV is shown as a function of time (results from spectral UV-radiative transfer calculation) for various values of the total column ozone for clear sky conditions on June 21, in The Netherlands. From this figure it can be seen that the DUV strongly depends on total column ozone, and also on the time of day, or equivalently, solar elevation.

## 1.4 Impact of Other Parameters on Ultraviolet Radiation

### 1.4.1 Solar elevation

Ozone is the parameter best known to affect UV-radiation in the atmosphere. It is, however, not the most important one. During winter, and also in summer in the morning and the evening, it is mainly the solar elevation (defined as the angular distance of the Sun above the horizon) that determines the amount of UV at the Earth surface. At low solar elevations the path length for radiation traversing through the atmosphere is so long that most of the UV is absorbed before it can reach the Earth surface. In Fig. 1.6 the DUV is shown as function of total ozone for solar elevations (se) of 20, 30, 40, 50, and 61.3°. For all total ozone values, DUV strongly depends on solar elevation.

In Fig. 1.7 all DUV measurements recorded in the period January–September 1994 are shown as a function of solar elevation. These measurements thus include all kinds of possible cloud cover conditions, i.e. from clear skies to completely overcast conditions. From this figure it can be seen that for a certain solar elevation almost every value for the DUV is

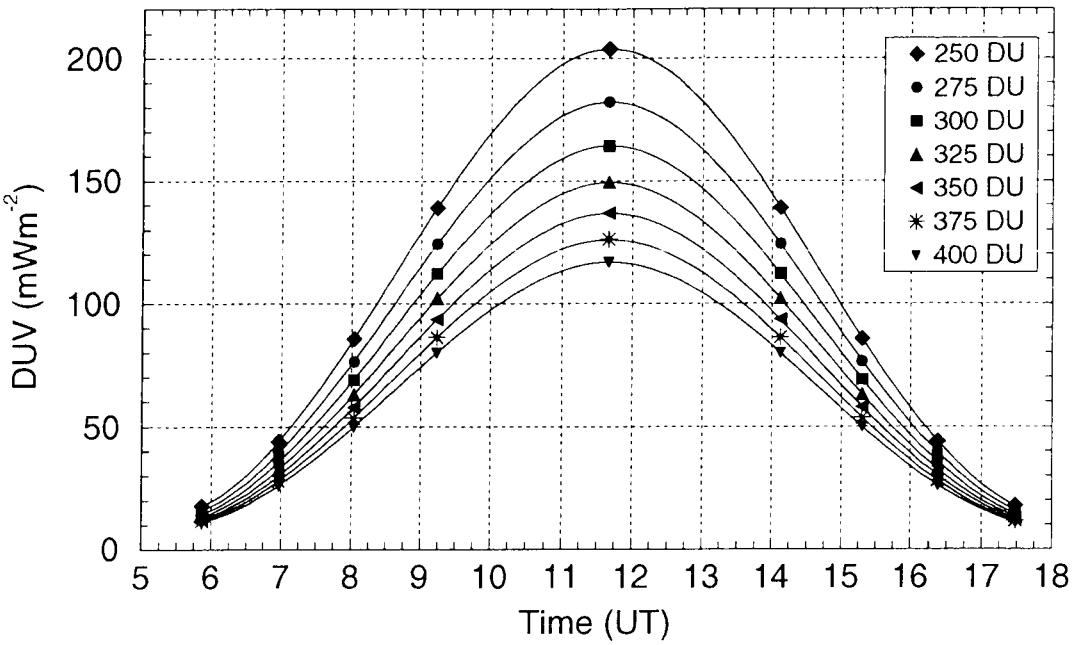


**Figure 1.5** DUV as a function of time for The Netherlands, June 21, clear sky conditions, and various values of total columns ozone (from spectral UV-radiative transfer calculations).

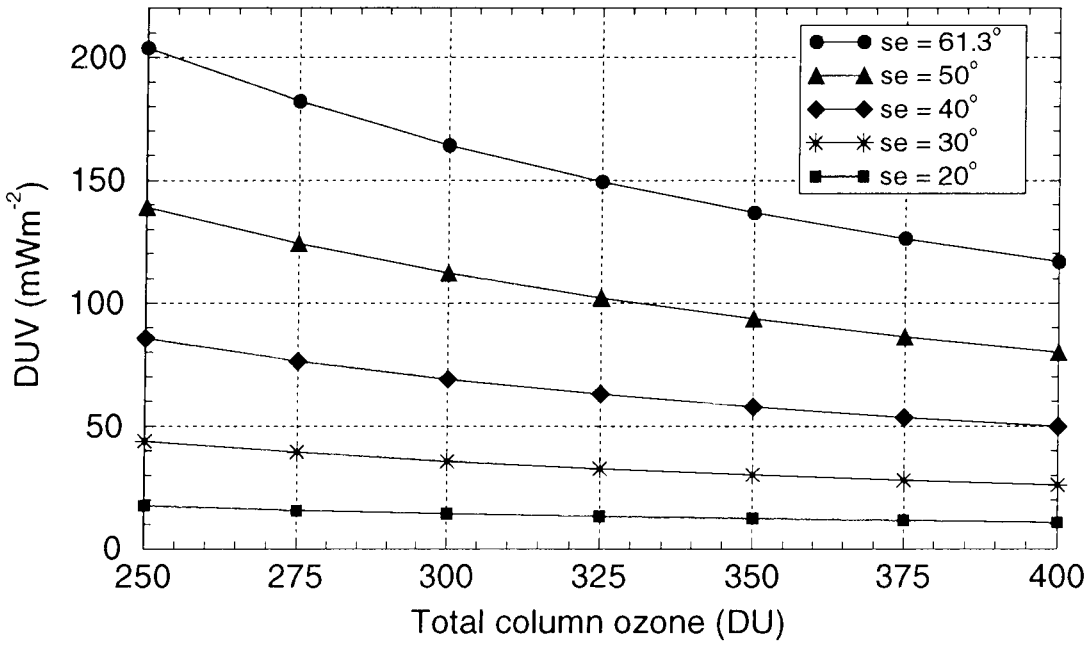


**Figure 1.6** DUV as a function of total column ozone for various solar elevations. The atmosphere model used in the calculations was the same as that used for Fig. 1.5.

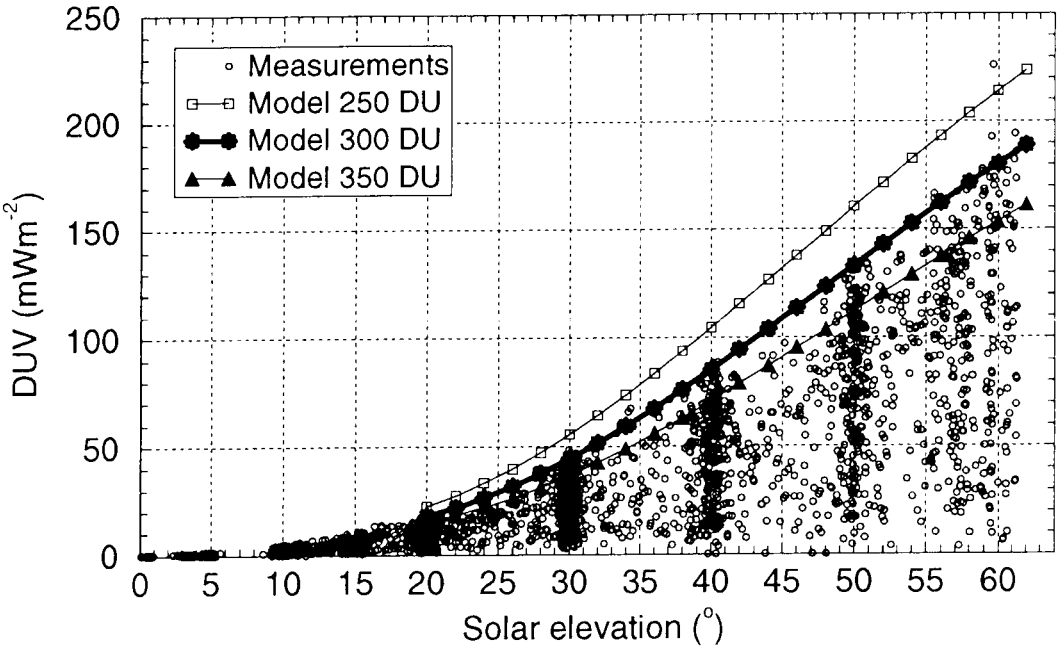


**Figure 1.7** All DUV-measurements from January to September 1994, as a function solar elevation. The curve that agrees best with the maximum observed values is computed with Eq.(1.10) using total column ozone of 300 DU.

possible within a certain envelope. In the same graph three curves are shown. These were computed employing an empirical model that uses total column ozone and solar elevation as input (see Sect. 1.4.2, Wilson *et al.* 1992; Kerr *et al.* 1994). For the Netherlands the maximum value for the DUV can be approximated using this model with a total column ozone of 300 DU.

### 1.4.2 Clouds

Spinhirne and Green (1978) first investigated effects of clouds on UV-radiation using radiative transfer calculations. The only case they could study was that for homogeneous cloud layers (broken clouds today still pose a big problem for radiative transfer modelling). Their main findings were *(i)* that for $\lambda < 300$ nm absorption due to tropospheric ozone is sensitive to cloud height and ground albedo, and *(ii)* for increasing cloud optical depth, UV-transmission decreases less than transmission of the total solar radiation. More recently, Stamnes *et al.* (1990) used spectral irradiance measurements and model calculations to derive 'equivalent' stratified cloud optical depths. In 1990 Frederick and Snell (1990) found from analysis of Robertson-Berger meter data that the annual mean erythemal irradiance is reduced between 22% and 38% relative to the clear sky value by clouds. Furthermore, they concluded that variations in cloud optical depth within 10%, have less impact on surface level UV-irradiances than changes in fractional cloud cover. Lubin and Frederick (1991) combined spectral UV-measurements and radiative transfer calculations to study the impact of clouds at Palmer Station, Antarctica (64°46'S, 60°04'W). They reported that for the 'average overcast sky' for this region UV-irradiances were slightly higher than 50% of the

clear sky values; for the largest cloud optical depths this reduced to 20%. Tsay and Stamnes (1992) considered the impact on UV-transmission of various cloud types that prevail in the summertime Artic, using radiative transfer calculations. Their most important conclusions are that stratus clouds and Artic haze tend to decrease UV-surface levels, whereas stratospheric aerosols imply an increase of ground level UV-irradiances. Bais *et al.* (1993) studied the effect of cloud cover on UV-transmission for a solar zenith angle of 50° for Thessaloniki, Greece (40°N), using spectral UV-measurements. They derived an empirical relation to compute DUV as a function of cloud cover [1], i.e.

$$DUV = 1 + 0.06cl - 0.02cl^2, \tag{1.9}$$

where $cl$ is the cloud cover (valid for $3 < cl < 8$). Furthermore, they found a decrease up to 80% in the UV-irradiance relative to the clear sky values for completely overcast conditions.

DUV measurements recorded at the KNMI with the Brewer during the first eight months of 1994, are depicted Fig. 1.8 as a function of cloud cover. The measurements are normalized using maximum values for clear sky conditions that were obtained from an empirical model (Wilson *et al.* 1992; Kerr *et al.* 1994). The relation that was used to calculate the maximum clear sky DUV is given by

$$DUV = \cos\theta_0 \mathrm{e}^{A+B\frac{X}{\cos\theta_0}+C\frac{1}{\cos\theta_0}+D\left(\frac{X}{\cos\theta_0}\right)^2+E\left(\frac{1}{\cos\theta_0}\right)^2}, \tag{1.10}$$

where DUV is the weighed integrated UV-irradiance in $\mathrm{mWm}^{-2}$ [cf. Eq.(1.1)], $\theta_0$ is the solar zenith angle, $X$ is the total column ozone in cm at STP (i.e. DU$\times 10^{-3}$). The constants $A = 7.093$, $B = -3.927$, $C = -0.636$, $D = 1.525$ and $E = 0.1183$ have been determined from a least square fit. Only solar zenith angles smaller than 20° are used for the model calculations. Because both the solar elevation and ozone are taken into account in this model, the normalized measurements are independent of these parameters.

There are several interesting features in Fig. 1.8. For 0/8th cloud cover all ratios are within the interval 0.8–1.1. The model does not take into account effects of aerosol, haze, ground albedo, UV-absorption by $SO_2$, and all other parameters that may influence ground level UV-irradiance for clear sky conditions. The magnitude of the fluctuations in the normalized DUV thus demonstrates that variations in UV-irradiances up to 20% can be expected for a given solar elevation and total column ozone.

It can be seen from this figure that the highest values for the DUV do not occur for clear sky conditions, but for situations with 1/8th to 6/8th cloud cover. This effect is caused by reflections at the side of clouds. When (cumulus) clouds are located near the position of the Sun in the sky, a large amount of almost direct solar radiation can be reflected in the direction of the detector. The amount of observed global UV-radiation can then increase beyond values measured under clear sky conditions (McKenzie *et al.* 1991; Mims III and Frederick 1994).

[1] A meteorological parameter for clouds is *cloud cover*. It describes the fraction of the overhead sky covered by clouds in eighths. Zero/eighth means a cloudless sky, whereas eight/eighth means completely overcast.

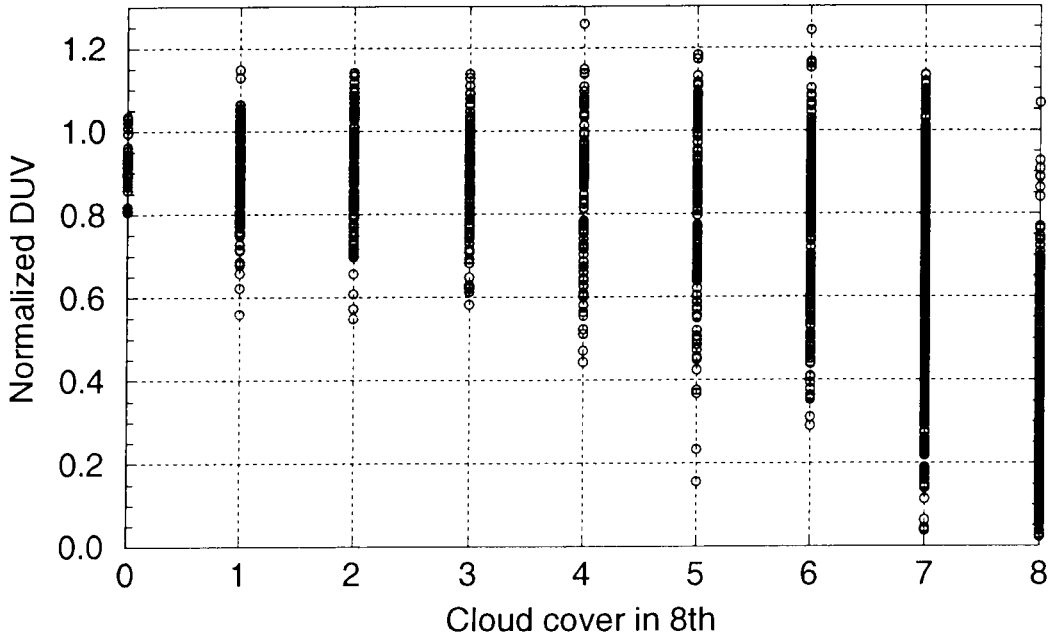


**Figure 1.8** Normalized DUV as a function of cloud cover for the period January–September 1994.

For increasing cloud cover, the spread of the measurements also increases, especially towards lower values of the normalized DUV. This means that for high cloud cover virtually all possible values of DUV can be measured, from 25% extra compared to clear sky conditions to approximately 0. The maximum amount of DUV was observed for a cloud cover of 4/8th.

This increase in irradiance in the presence of cumulus clouds is also observed in measurements of the narrow band and the short wave (broad band) instruments. In Fig. 1.9, 10-minute averaged measurements of the global radiation (pyranometer, $300 \lesssim \lambda \lesssim 3000$ nm), and the UVA and UVB-global instruments are shown (specifications of the narrow band UVA and UVB instruments are discussed in Chap. 2). The dash-dotted curves represent measurements for July 12, 1994, for clear sky conditions. The solid lines are measurements for partly clouded conditions on June 28, 1994. Between 11:00 UT and 14:00 UT (June 28) cloud cover varied between 1/8th and 5/8th. This resulted in an increase of the global radiation of 38%, and approximately 15% for both the UVA and UVB global measurements, relative to the clear sky measurements. A reason for the larger increase of the broad band global radiation is a wavelength effect. The UVA and UVB sensors measure at wavelengths centered around 367 and 306 nm, respectively. Rayleigh-scattering is proportional to $\lambda^{-4}$, i.e. the shorter the wavelength of the radiation, the more effective it is scattered in the atmosphere. The contribution of the direct solar beam to global radiation will therefore be larger in the visible and infrared wavelength region than in the UV, simply because most of the UV-radiation has already been scattered out of the direct solar beam before it reaches tropospheric clouds and the Earth surface, although Tsay and Stamnes (1992) found an increase of ground level UV-irradiance when aerosol was present.

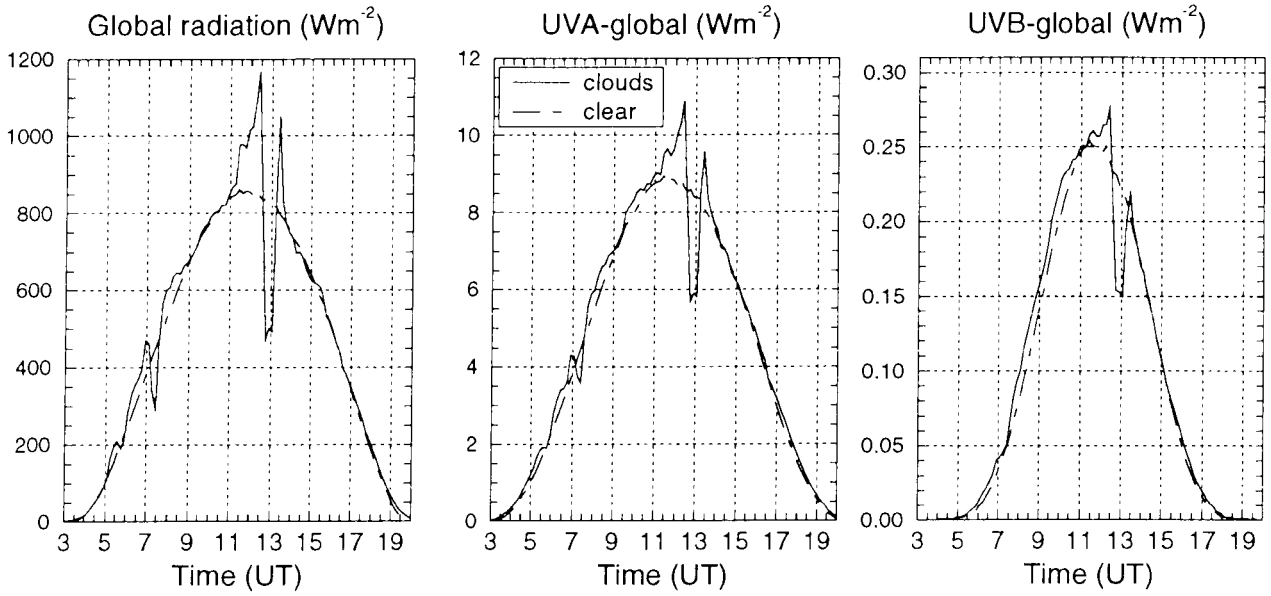


**Figure 1.9** Broad band global radiation, UVA global radiation, and UVB global for June 28, 1994. The sharp increases in radiation relative to the clear sky measurements (July 12, 1994) are caused by reflection of solar radiation at the side of cumulus clouds.

### 1.4.3 Aerosol

Aerosol can affect ground level UV-irradiances in a direct and indirect manner. Direct influence takes place by reflection of radiation back into the higher parts of the atmosphere. This process simply causes less radiation to reach the Earth surface. Indirect effects can take place through several mechanisms. Aerosol particles act as cloud condensation nuclei. Cloud formation can thus increase when much aerosol is present in the atmosphere, and in the previous section effects of clouds on UV-transmission have been discussed. Another indirect effect is that atmospheric aerosol can cause large disturbances in stratospheric ozone chemistry, usually resulting in ozone depletion. A well known opportunity to investigate aerosol effects was provided by the eruption of Mt. Pinatubo (Philippines) in June 1991. Many researchers reported large decreases in stratospheric ozone amounts, especially in the Antarctic spring (see e.g. Brasseur 1992; Kerr 1993). Although the Mt. Pinatubo eruption was initially not accepted by all atmospheric scientist to be the cause of global ozone depletion, according to the new WMO/UNEP Ozone Assessment report (1994), there is more consensus now.

From a comparison of the narrow band UV-measurements in De Bilt for February 1992 and 1993, it was observed that the 1993 levels were substantially higher than the 1992 levels (KMI *et al.* 1993). As a (partial) explanation this phenomenon was ascribed to lower ozone values in 1993, which in turn was assumed to be caused by Mt. Pinatubo aerosol.

## 1.5 UV-forecasts

Exposure of human skin to ultraviolet radiation can cause sunburn, various kinds of skin cancer, and other health risks (Van der Leun 1994). Moreover, in the Western world an increase in exposure is observed over the last few years. This is mainly caused by human behaviour: it is fashionable to have a sun tanned skin.

In 1994 the Netherlands Cancer Association (KWF) started a campaign to make the Dutch people more aware of UV-related health risks. One of the key-issues of the campaign is that some simple changes in the human behaviour can reduce the risks for our skin considerably. KNMI can play a important role in this campaign. At KNMI there is 150 years of experience in issuing warnings about weather related risks. This service can easily be extended with forecasts on exposure to ultraviolet sunlight. People are interested in forecasts of warm and sunny weather in the summer season. If during the summer in the daily weather forecast a forecast of the amount of ultraviolet radiation is included (e.g. in the form of an *index*), it will reach a large audience, and be a valuable contribution to the KWF-campaign.

In this section the forecasting system is discussed, and a first analysis of forecasts compared with measurements is given. For a more extensive treatment see Allaart (1994b). At this point it is emphasized that the discussion whether or not, and when KNMI will start issuing UV-forecasts is still going on, and no decisions has been made on the subject yet.

### 1.5.1 What is forecasted?

In Sect. 1.2 DUV was introduced as the weighed integrated UV-irradiance in $\mathrm{mWm}^{-2}$ (cf. Eq.(1.1). To convert DUV to an index between 0 and 10, it is divided by 25. The so obtained index is called *Solar Power* ('Zonnekracht' in Dutch), and can easily be translated into 'time to burn'.

This index was originally developed in Canada, and most countries that issue UV-forecasts are using it nowadays. At a WMO meeting on UVB-radiation and UV-forecasts in July 1994 (Les Diablerets, Switzerland), it was recommended that meteorological stations that are issuing UV-forecasts or who are planning to start, use this index (additional information is optional).

### 1.5.2 Forecasting DUV

Some parameters that affect ground level UV can be predicted by meteorologists. Others are so local that it is impossible to include them in the prediction. Clouds are an intermediate case. Large cloud decks, for example those associated with frontal zones, can be predicted. Smaller clouds, e.g. those associated with unstable air, are notoriously difficult to predict. It is also impractical to include their presence –other than in statistical terms– in the daily weather forecast. Therefore, a forecast is made giving the index for clear sky and partially cloudy conditions.

For accurate computations of DUV as a function of various atmospheric parameters

and solar elevation, a radiation transfer code with an atmosphere model should be used. Although such a code is available, for daily forecasts it is impractical to use, because radiative transfer computations are complicated and expensive. Reasonable results are also obtained with the Canadian model, i.e. employing Eq.(1.10). (Wilson *et al.* 1992; Kerr *et al.* 1994). Model calculations show reasonable agreement with measurements (see Fig. 1.11), but more data (i.e. clear sky days) are needed to tune the model.

### 1.5.3 Predicting total column ozone

Variations in total column ozone are dominated by variations in the amount of ozone in the lower stratosphere. Several methods are in use to predict total column ozone in the lower stratosphere. They all depend on either advection of ozone with an appropriate wind, or correlation of ozone with other atmospheric quantities.

The method used at KNMI uses of a correlation between total column ozone and column integrated potential vorticity. A discussion of this correlation is given by Allaart *et al.* (1993). Essential in this method is the fact that on a hemispheric scale the relation

$$O_3 = \kappa \ \mathrm{TPV} + \lambda \tag{1.11}$$

holds, where $O_3$ is total column ozone as measured by the TOVS (TIROS operational Vertical Sounder) instrument on board the NOAA operational meteorological satellites. TPV is the column integrated potential vorticity, and $\kappa$ and $\lambda$ are slowly varying parameters.

TPV is calculated from predicted fields from the General Circulation Model (GCM) of the European Centre for Medium- Range Weather Forecasts (ECMWF). For practical reasons the vorticity fields are calculated from the wind fields. Computation of TPV from the vorticity and temperature fields is described in Allaart *et al.* (1993). The method works as follows.

1. Calculation of yesterday's ozone field. Atmospheric temperatures are measured by the TOVS instruments. These data are received at KNMI for the European and North Atlantic region. From these temperatures total column ozone is computed employing an algorithm developed by Cariolle (Lefèvre *et al.* 1991). The data for one day are averaged, and mapped onto a grid. The measurements carried out near noon are given the highest weighing factor.

2. From yesterday's ozone and (stored) TPV fields, yesterday's $\kappa$ and $\lambda$ are computed. Special care is taken to prevent the difference between the current values and earlier values to become too large, to ensure that one day of incorrect observations will not upset the system.

3. From the new ECMWF forecast TPV fields are calculated for the next three days. For practical reasons the special HIRLAM or 00-hour run of the model is used. Because we are interested in the noon UV flux, only forecasts for +12 hours (today), +36 hours

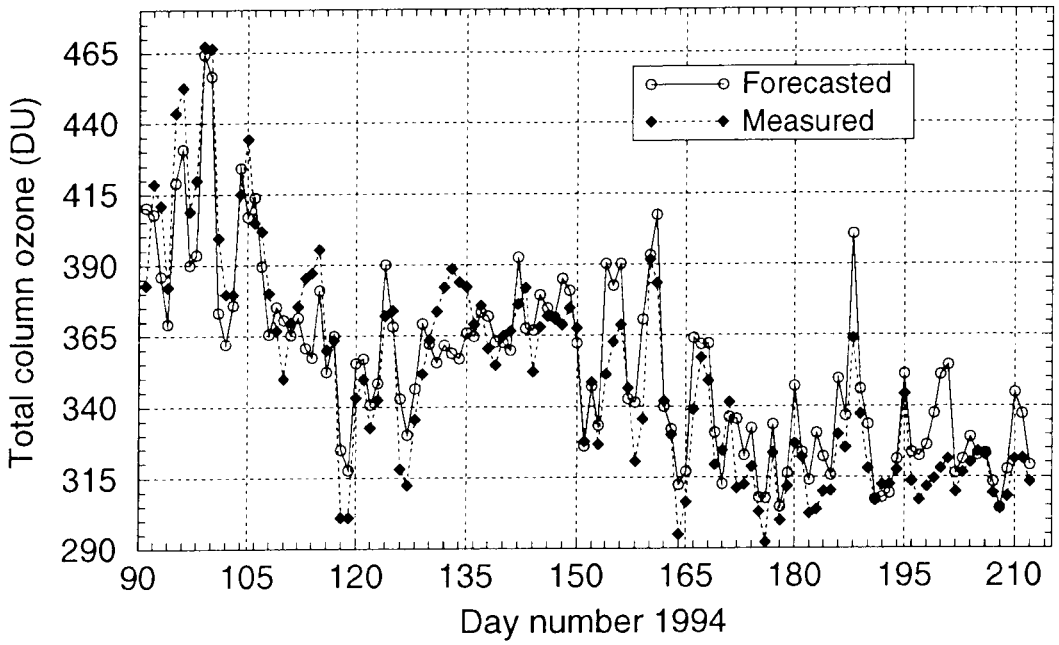


**Figure 1.10** Measured and forecasted total column ozone for the period April-July 1994.

(tomorrow) and +60 hours (day after tomorrow) are computed. The computed TPV fields are stored for use during the next days.

4. From the forecasted TPV fields and yesterday's $\kappa$ and $\lambda$, a forecast for the ozone field is calculated. Because both $\kappa$ and $\lambda$ vary slowly in time, the error introduced by using yesterday's values is negligible.

5. The solar elevation at noon is calculated, and with aid of the Canadian model and the predicted ozone field, the noon DUV flux is calculated, which, divided by 25 gives the index.

In Fig. 1.10 forecasted and measured total column ozone are compared. It can be seen from this figure that except for a few brief periods in time, the forecasts and measurement show good agreement. Allaart (1994b) gives a preliminary qualitative discussion of how good the forecasts are compared with TOVS and Brewer measurements. The conclusion is that the forecasting method shows a clear skill of 29% over 'persistence', i.e. using the measured total column ozone of the previous day as forecast for the next day.

Figure 1.11 shows both the predicted and the daily observed maximum DUV as a function of day number for 1994. In the curve for the forecasted DUV effects of variations in total column ozone are represented by the small scale structure. The large variations in the curve representing measured DUV are mainly caused by clouds. Note that the forecasted DUV are local solar noon values, whereas the measured DUV are daily maxima. They do not necessarily are local solar noon measurements, especially if clouds are present.

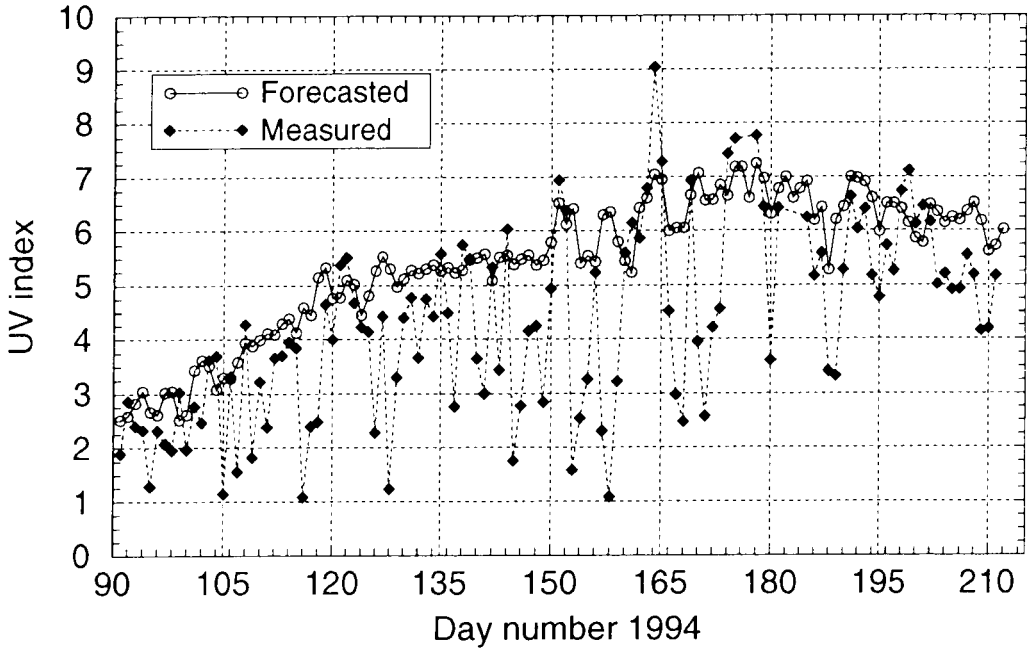


**Figure 1.11** Forecasted DUV for clear sky conditions, and measured DUV for the period April-July 1994. Clouds are the main cause of the large variations in the measurements.

## Acknowledgements

The work described in this report has been supported by NOP (project no. 852088), KNMI, and EU (STEP project 76). Wout Slob kept on coming to the KNMI for half a year after his retirement to help out on all issues concerning solar radiation measurements. Mark Allaart provided the text and figures for the section on UV-forecasts. Piet Stammes kindly made his radiative transfer code available. He, and also Wiel Wauben, continuously made improvements in the code, removed several bugs, and patiently explained everything about radiative transfer calculations that was needed to perform the computations. Casper Hofman wrote data-acquisition software for several of the measurement instruments. Without the efforts and advice of Jaap Boot, Cor Schuurmans, Andre van London, Rob van Krimpen, Jan Middelkoop, Nanne de Jong, and several people from the KNMI-workshops, it would have been impossible to build the UV-calibration lab in the short time it has taken now.

# Chapter 2

# UV-Measurements and Calibrations

## 2.1 Introduction

In this chapter a description and the specifications of the instruments that are used for the UV-research at the KNMI are given. Some instruments used for auxiliary measurement, e.g. broad band radiation meters, are also briefly described. Section 2.3 is devoted to the diode array instrument. This is (not yet) an operational monitoring instrument, but it is used for experimental research. This instrument has participated in two international UV-instrument intercomparisons (Gardiner and Kirsch 1993, 1994), and some results of its performance will be shown.

The instruments discussed in this chapter perform three types of measurements. The first is the so-called *global* measurement. All instruments doing global measurements have in common that they collect radiation from the hemisphere above it. The well known pyranometer (e.g. the Kipp & Zonen CM-11) that measures solar radiation between approximately 300 and 3000 nm, is such an instrument. Since it records all radiation that enters the detector through a horizontal plane, it measures an *irradiance*, also called *flux*. The second kind of measurement is called *direct* solar radiation measurement. In this case the instrument is looking into the direction of the Sun, measuring the energy flux of the direct solar beam. Such instruments measuring broad band solar radiation are called pyrheliometers (e.g. the Kipp & Zonen CH-1). If the instrument is used for monitoring purposes it must be mounted on a solar tracking device, since at all times during the day it must remain pointed at the Sun. WMO standards prescribe an opening angle of 5° around the solar disk for direct solar measurements. The third type of measurement is the so called *diffuse* measurement. It basically is the same measurement as the global measurement, but now with the solar disk obscured by a shadow disk or band. If the disk is used, a solar tracker is required, because the sensor should remain in the shade of the disk while the Sun moves across the sky. The disk should have a size that obscures the Sun with the same opening angle as the direct solar measurements, i.e. 5°. In this case the relation

$$G = Dif + \cos\theta_0 Dir \tag{2.1}$$

holds, where $G$, $Dif$, and $Dir$ are global, diffuse and direct radiation ($\mathrm{Wm}^{-2}$), respectively, and $\theta_0$ is the solar zenith angle. This relation is particularly useful for validation of the measurements.

## 2.2 Brewer Photospectrometer #100

The Brewer photospectrometer was originally built by a Canadian company called Sci-Tec to measure total column ozone. The first instruments became operational in the beginning of the eighties. It basically consisted of a single monochromator and some entrance optics built into a weatherproof housing. Later on the instrument was fully automated, and the option to make scans of the UV-irradiance up to 325 nm was added.

The WMO collects ozone measurements from all over the world. Originally, the ground based measurements were provided by Dobson photospectrometers. These instruments are, however, not weatherproof, and are operated manually (causing missing data during weekends, and on all other occasions when operators were unable to perform the measurements). Since the introduction of the Brewer, they are gradually taking over from the Dobsons, and the WMO accepts the Brewer ozone data as good and reliable. At the moment approximately 120 Brewers are operational at locations spread all over the entire globe.

When it became clear that in single monochromators stray light poses a problem for UV-scans starting below 300 nm (the most interesting region for absorption by ozone and biological studies), a new version of the Brewer with a double monochromator was developed, the Brewer MK III. This new version also had the possibility to do 'extended UV-scans', i.e. scans from 286.5 nm to 364.5 nm. It was extensively tested in an European UV-instrument intercomparison (Gardiner and Kirsch 1994), where it performed very well. At this time already four Brewers (MK III) are operational, and more will follow. The Brewer that was purchased by the KNMI in 1993 was the second operational MK III. Purely by coincidence it was also Brewer #100.

Brewer #100 was installed on top of the KNMI-roof in December 1993. During this month its operation was tested, which was necessary after shipment from Canada. Monitoring of ozone and UV-radiation started January 1, 1994.

### 2.2.1 Ozone measurements

Under clear sky condition the amount of atmospheric ozone can best be determined from measurements of the extinction of the direct solar UV-radiation. The basic equation describing this process is (Kerr *et al.* 1985)

$$I_\lambda = I_{\lambda 0} \exp\left(-\beta_\lambda m_\beta - \delta_\lambda m_\delta - \alpha_\lambda O3 \mu_{O_3} - \gamma_\lambda SO_2 \mu_{SO_2}\right), \tag{2.2}$$

where $I_\lambda$ is the measured flux, $I_{\lambda 0}$ is the flux at the top of the atmosphere, $\beta_\lambda$ is the Rayleigh scattering coefficient, $m_\beta$ the airmass for Rayleigh scattering, $\delta_\lambda$ and $m_\delta$ the scattering coefficient and airmass, respectively, for aerosol scattering, $\alpha_\lambda$ the ozone absorption coefficients, $O_3$ the total column ozone, $\mu_{O_3}$ the airmass for ozone, $\gamma_\lambda$ the $SO_2$ absorption coefficients, $SO_2$ the total column sulphur dioxide, and $\mu_{SO_2}$ the airmass for $SO_2$. The $\lambda$ indicates that all quantities are wavelength dependent. The Brewer uses four wavelengths for ozone measurements: 310.1 nm, 313.5 nm, 316.8 nm, and 320.1 nm. Taking the ratios of the measured fluxes for these wavelengths, the influence of aerosol ($\delta_\lambda m_\delta$) and $SO_2$ ($\gamma_\lambda SO_2 \mu_{SO_2}$) can be

eliminated. The extraterrestrial $I_{\lambda 0}$ has to be determined for the four wavelengths from Langley-plots, which is the calibration of the instrument. All other quantities are known or can be computed, and finally $O_3$ can be determined. This type of measurements is called a *Direct Sun (DS)* measurement.

There is an additional wavelength at which $I$ is measured: 306.3 nm. This wavelength coincides with a maximum in the absorption spectrum of $SO_2$. After the amount of ozone has been determined, the total column $SO_2$ can also be found using this extra wavelength together with the measurements at 316.8 nm and 320.1 nm (see e.g. Kerr *et al.* 1985).

Under cloudy conditions *zenith sky (ZS)* measurements are performed to obtain the total column ozone. From a comparison of DS and ZS measurements on clear sky days, a ten parameter fit is made to compute the total column ozone from the ZS measurement. The Brewer instruments initially operate with a standard fit supplied by Sci-Tec, but after a year of measurements the coefficients should be computed anew. From all 1994 measurements we observed that the ZS and DS measurements for clear sky conditions usually agreed within 1%.

According to the manufacturers of the Brewer the accuracy of the DS measurements is better than 1%, and that of the ZS measurements better than 10%, depending on how good the fit agrees with the DS values. From our observation we conclude that the ZS measurements have an accuracy of better than 5%. The stability of the ozone calibration is checked several times per day with an internal tungsten halogen lamp. Wavelength calibrations are also performed a number of times per day using an internal mercury lamp.

### 2.2.2 Spectral UV-measurements

The Brewer is equipped with two Ebert-type monchromators, which are placed on top of each other. The dispersive components are two plane holographic gratings, having 3600 lines/mm each, which are operated in the first order. A scan starts at 286.5 nm and goes up to 364.5 nm, and takes about seven minutes to complete. Measurements are controlled by a computer, which is also used for the data acquisition. On top of the weatherproof housing in which the instrument is placed, there is a quartz dome with a teflon diffuser underneath it. The Brewer thus measures spectral UV-irradiances. It is also possible to perform scans of the direct solar UV, but the instrument has not yet been calibrated for this purpose. This will be done in the near future. For a more complete instrument description and its performance, we refer to Kerr *et al.* (1985), and Gardiner and Kirsch (1994).

The irradiance calibration was performed by Sci-Tec, i.e. the instrument was calibrated in Canada before it was shipped to KNMI in December 1993. In August 1994 Brewer #100 participated in a small scale intercomparison in Bilthoven, with the RIVM and Austria-Innsbruck instruments (cf. Gardiner and Kirsch 1994). From this intercomparison we learned that the irradiance calibration provided by Sci-Tec produced approximately 20% too low UV-readings. All results shown in this report have been corrected for this, and with the recent completion of the UV-calibration laboratory at the KNMI we are able to perform a new calibration. Field calibrations are performed with small 50 W lamps every two weeks

**Table 2.1** Technical specifications of the double monochromator Brewer and the diode array instrument.

| | Brewer #100<br>MK III | Diode array<br>EG&G M1229 |
|---|---|---|
| Focal length (mm) | 160 | 156 |
| Gratings | two | one |
| type | plane holographic | plane ruled |
| lines/mm | 3600 | 1200 |
| Spectral range (nm) | 286.5–364.5 | 290–430 |
| Wavelength increment (nm) | 0.5 | 0.13 |
| Bandwidth (FWHM) (nm) | 0.6 | 0.8 |
| Scan duration | 7 min | 3 sec |
| Detector type | photomultiplier<br>EMI 9789QA | diode array 1024 elements<br>M1453A |
| Diffuser | teflon plate | teflon plate |
| Weatherproof | yes | no |
| Automatic | yes | no |
| Temperature stabilized | | |
| optics | yes | no |
| Stray light removed | optional | yes |
| Calibration standard | NIST | NIST |
| Main lamp | 1000 W DXW | 1000 W FEL |
| Secondary lamp | 50 W | 200 W |

to monitor the stability of the instrument. Furthermore, the Brewer will be taken into the lab every two months to do a new irradiance calibration with a calibrated 1000 W DXW lamp. If the instrument proofs to be stable enough, this may be reduced to once per three or four months. Wavelength calibrations are performed with the internal mercury lamp several times per day, especially when temperature changes occur.

In Table 2.1 some specifications of the Brewer MK III are given, together with specifications of the diode array instrument that is discussed in the next section.

## 2.3 Diode Array Instrument

By using a diode array as detector, the OMA (Optical Multichannel Analyser) obviates the need for a scanning mechanism and gathers the whole spectrum at once. A great advantage is that measurements are not affected by short term weather changes such as passing clouds.

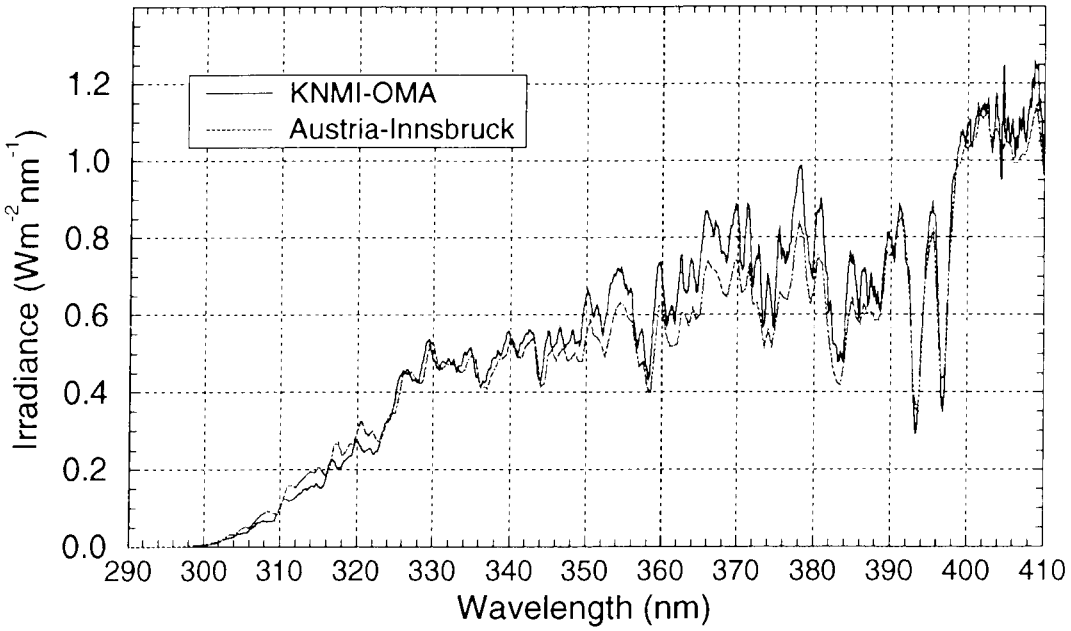


**Figure 2.1** UV-irradiances measured with the KNMI-OMA and the Austria-Innsbruck scanning double monochromator.

Recording a UV-spectrum takes between 0.3 and 18 seconds for clear sky high sun and overcast low sun conditions, respectively, whereas a scanning instruments needs at least several minutes. A disadvantage is that the spectrometer is a single monochromator, and therefore stray light is a considerable problem that has to be eliminated or corrected for.

The monochromator of the OMA is the Jarrell Ash MonoSpec 18, which is based on a crossed Czerny-Turner spectrometer, and it is operated with a 1200 lines/mm grating in the first order. The detector is a Reticon 1024-element diode array behind a fused silica plate. The array measures 25 mm $\times$ 2.5 mm, and it is Peltier cooled to 5° C.

The instruments measures global spectral UV-radiation, usually between 290 and 415 nm. Stray light correction can be performed in different ways. In the 1993 instrument intercomparison in Garmisch-Partenkirchen, (Gardiner and Kirsch 1994) a filter was used that has a cut-off for wavelengths $\gtrsim$ 360 nm. This prevents most visual and infrared radiation from entering the spectrometer. The residual stray light is corrected for by subtracting the averaged signal measured by the first 20 diodes (290–292.5 nm), where no radiation should be detected.

The OMA participated in two European UV-instrument intercomparisons (Thessaloniki 1992, and Garmisch-Partenkirchen 1993, Gardiner and Kirsch 1993, 1994). In the last intercomparison the instrument performed well, as can be seen from Fig. 2.1. In this figure two UV-scans are shown (July 24, 1994, 12:48 UT). One was recorded with the KNMI-OMA, the other with the instrument that was used as reference throughout the campaign, the Austria-Innsbruck instrument operated by Blumthaler and Huber (Gardiner and Kirsch 1994).

For the 1995 European UV-instrument intercomparison (May 1995, Ispra, Italy) the

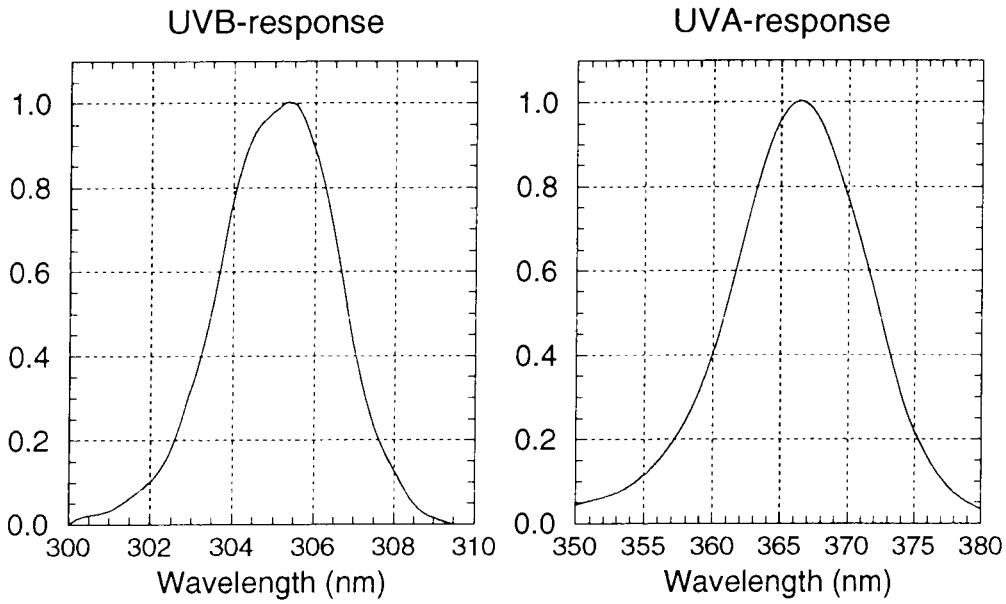


**Figure 2.2** Spectral responses of the UVB and UVA sensors (Kipp & Zonen 1994).

instrument will be improved in several ways. It will be built into a weatherproof housing, and the optics will be temperature stabilized. We are also considering to make it suitable for radiance measurement so that we can do zenith sky and direct sun measurements.

## 2.4 Narrow Band UV-meters

The narrow band UV-meters are filter instruments, i.e. the filter inside the instrument determines its spectral response. Two versions are currently in use at the KNMI

**UVB** This version operates at 306 nm, and the filter has a bandwidth (FWHM) of 3 nm. In this spectral region the irradiance varies strongly as a function of wavelength. To obtain a good correlation with spectral UV-measurements the choice was made for a narrow bandwidth.

**UVA** The UVA-instruments are equipped with a filter having a central wavelength of 367 nm, and a bandwidth (FWHM) of 10 nm. The spectral responses of both the UVB and UVA-sensors (as measured by Kipp & Zonen) is shown in Fig. 2.2.

The UVA and UVB sensors are used in global as well as direct solar radiation measuring devices. The 'final' versions are operational since March 1994. Some results were shown in Fig. 1.9.

The sensors are temperature stabilized at 40° C, because the interference filters are temperature sensitive. At this time the data are stored as ten-minute averages, including the maximum and minimum values that are recorded within these ten minutes. In the near future this will be changed so that *all* measurements are stored. This high frequency sampled data should provide better information on cloud cover than ten-minute averages.

Calibration of the instruments is performed with the 1000 W FEL lamp that is mentioned in Table 2.1. The spectral UV-measurements are used as an additional check for the irradiance measurements.

## 2.5 Additional Measurements

Additional radiation measurements consist of

**Global Radiation** Pyranometer measurements, i.e. measurements of global radiation between 300 nm and 3000 nm.

**Direct Radiation** Pyrheliometer measurements, also measurements of the direct solar beam, between 300 nm and 3000 nm.

**Diffuse Radiation** Measurements of the scattered component of the global radiation, same wavelength region.

These measurements are also stored on a ten-minute average basis, including the maxima and minima. They provide useful information on the weather conditions for each day of the year. Moreover, direct solar radiation measurements are sensitive to and provide information on aerosol and haze in the atmosphere (turbidity). Correlations between these measurements and the narrow band UVA, UVB, and spectral UV-measurements are still to be investigated.

Apart from the additional radiation measurements, in principle all meteorological data that is gathered by the Climatological Department of KNMI, is available for data analysis. Examples of this data are cloud cover, ozone profiles, radio sonde profiles of pressure, temperature and humidity.

# Chapter 3

# KNMI UV-Calibration Laboratory

## 3.1 Introduction

Irradiance calibrations of (spectral) UV-measurement instruments is a difficult task, especially in the UVB-region of the spectrum. The solar irradiance decreases by four to five orders of magnitude between 330 and 290 nm. A 1000 W FEL calibration standard lamp has rather flat spectral characteristics in this wavelength region, and most of the power that such lamps radiate is in the visible and infrared part of the spectrum. This means that the UV-instruments must have good stray light rejection properties, or they must have blocking filters (e.g. the diode array instrument with the single monochromator). However, it remains a problem that the spectral characteristics of calibration lamps are quite different from the solar spectrum. To gather long term reliable UV-measurements that can be used for trend analysis, the calibration of the measuring devices must be very good, stable, and reproducible. Therefore, a UV-calibration laboratory and the equipment used to perform calibrations must meet the highest standards.

In the spring of 1994 a start was made building a UV-calibration laboratory at the KNMI that meets these standards. The laboratory became operational in the autumn of 1994, and first tests and calibrations already showed good results. In this chapter a description of the new UV-calibration lab is given, and some of the instruments needed for calibrations will also be discussed.

## 3.2 UV-Calibration Laboratory

The KNMI-calibration laboratory measures 6.6 m $\times$ 5 m, and is large enough to contain an optical table and some additional experimental equipment. A schematic view of the laboratory is given in Fig. 3.1. The lab and some of its components are briefly discussed now.

### 3.2.1 Walls, floor, and ceiling

The walls, floor, and ceiling should reflect as little light as possible to avoid stray light to interfere with the calibrations. To achieve this, the walls and ceiling have been painted black. The floor is covered with a black velvet-like carpet, which is anti-static. The windows are covered with light tight black curtains. Everything else in the lab, including the furniture,

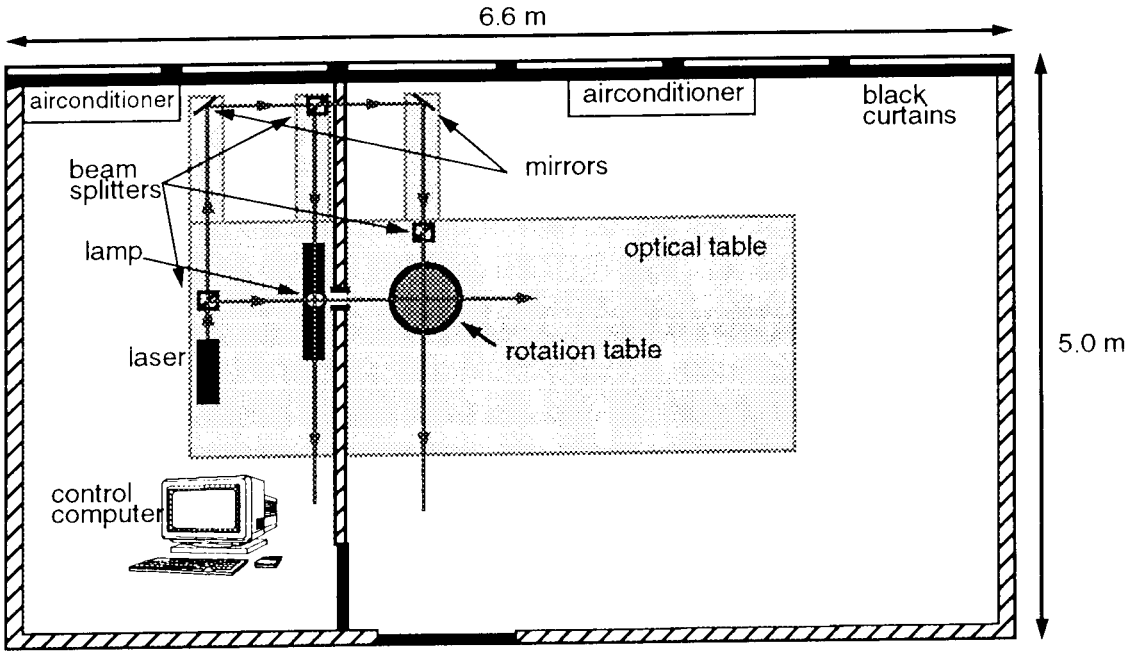


**Figure 3.1** Schematic top view of the KNMI UV-calibration laboratory. The construction holding the mirrors for the vertical laser beam is not shown.

is also black, or they are removed during calibrations.

### 3.2.2 Separation wall

The laboratory is divided into two separate rooms by a wall: the lamp and calibration rooms, respectively. The small lamp room (2.2 m × 5 m) is used to install the calibration lamp, the large calibration room is the room in which the actual calibration takes place. The two rooms are connected through a door, which is closed during calibrations. The only other connections between the two rooms are circular holes with diameters of 10 cm. One of the holes is intended to let the light of the calibration lamp enter into the calibration room to the instrument that must be calibrated. This way only a limited amount of the light enters the actual calibration room, reducing stray light considerably. The other hole is used only during the alignment of the instrument to be calibrated. For this alignment two laser beams enter the calibration room through the holes in the wall. The laser alignment will be discussed later.

### 3.2.3 Airconditioning

Most UV-instruments contain optical components and detectors that are sensitive to temperature changes. To avoid inconsistencies in calibrations that are performed at different moments in time, the temperature during calibrations should always be the same. This is achieved by employing two airconditioners. One of them is in the lamp room, the other in the calibration room. Moreover, 30 cm above the calibration lamp an exhaust hood removes the ozone created by UV-radiation of the lamp, and provides an air flow over the lamp having the constant room temperature.

## 3.3 Calibration Equipment

### 3.3.1 Calibration lamps

In the scientific UV-community only a few types of lamps are considered acceptable as primary UV-calibrations standards. They are 1000 W Quartz Tungsten Halogen (QTH) lamps, producing a modest amount of UV-radiation. For calibrations with the lamp in a vertical position and a horizontal beam, the FEL-type of lamp is used. For such calibrations the instrument to be calibrated must be turned on its side (in normal operating position it is usually looking vertically up). One must, however, be sure that rotating the instrument for the calibration does not affect its operation in any way.

In case the instrument cannot be turned on its side, e.g. the Brewer spectrophotometer, it must be calibrated employing a lamp vertically above the entrance optics of the instrument, with a vertical lamp beam. The FEL-lamps cannot be used in this position, but the so-called DXW lamps are available for vertical calibrations.

Both lamp types are present in the KNMI-laboratory (two FEL and one DXW). Since the calibration of such lamps is valid for only 50 hours, extra lamps must be purchased every year, and using our own spectrometers, the 'old' lamps can be recalibrated. They can then still be used for secondary (stability) calibrations and cosine response measurements.

### 3.3.2 Power supply

The 1000 W FEL and DXW lamps both operate at 8 A (110 V DC). The current going through the lamp during the calibration must be stable within 1 mA. To achieve this we use the OL83A Programmable Power supply (Optronics), that was especially developed for lamp calibration purposes. It is controlled by a PC, which at the same time records the lamp current and voltage during the calibration. In series with the lamp there is a high accuracy resistor (shunt) of 0.1 $\Omega \pm 10^{-6}\Omega$ (Gigahertz Optik). The voltage drop over this resistor should be 0.8 V $\pm$ 0.0001 V for a current of 8 A. This voltage is also monitored during a calibration, and is considered more reliable than the internal current and voltage measurements of the OL83A. The power supply performed well during the tests and the required current accuracy is achieved.

### 3.3.3 Optical table

A passively damped optical table (Melles Griot), measuring 3 m $\times$ 1.5 m, with a black top holds all the calibration equipment. The whole table top has M6 holes at 25 mm apart, to install optical components on it. Three matrix plate extensions (with the same M6-hole pattern) are mounted at the side of the table, which hold optical components that are used for the pre-calibration instrument alignment. During the test phase it was observed that if an instrument was aligned properly, overall vibrations and movements of the table do not influence the alignment at all. Only if, for example, a little pressure is exerted on one of the individual matrix plates, misalignment occurs.

### 3.3.4 Rotation table

Instruments that record global radiation must have a good cosine response. This means that if a parallel beam of light is incident on the detector, only the vertical downward component should be measured. If the parallel beam is incident at an angle $\theta$ with respect to the normal of the detector surface, the recorded signal thus should read $I_0 \cos\theta$, where $I_0$ is the detected signal for $\theta = 0$. If the deviation from the ideal cosine response is large, the measurements must be corrected using radiative transfer calculations, or the instrument response has to be improved. The cosine response is an important instrument characteristic, and it should be known for all global radiation measuring devices, spectral as well as band instruments.

There is a rotation table present in the calibration lab to measure cosine responses of global radiation instruments. Its angular accuracy is approximately 0.1°, which is more than sufficient to do good cosine response measurements. This rotation table is in the first place intended for operation with FEL-lamps, i.e. with a horizontal beam of light. However, to extend the functionality of the lab, the rotation table will be adapted to perform cosine response measurements with DXW-lamps and a vertical lamp beam.

### 3.3.5 Alignment procedures

Alignment of the instruments that are calibrated is very important. Observed ozone trends in our region are in the order of fraction of a percent per year. UV-trends will therefore be of the same order of magnitude. To be sure that detected UV-trends are really trends and not calibration inconsistencies, the calibrations must be very well reproducible.

The distance instrument–lamp, horizontal and vertical alignment of the detector surface, and the position of the lamp with respect to the instrument, must be reproducible for each new calibration (also the conditions in the calibration and lamp room, as discussed previously).

To achieve this reproducibility, a three-dimensional alignment procedure was developed employing a HeNe-laser, three beam splitters, and some mirrors. In Fig. 3.1 the horizontal alignment component is shown.

One laser beam passes through the lamp, and produces a spot at the position in space where the center of the detector must be placed. A second laser beam is also going through the lamp, but from the side. Parallel to this second beam is a third beam in the calibration room on the other side of the wall. This beam crosses the first beam at the center of the detector, and the distance between this beam and the parallel beam in the lamp room defines the distance instrument–lamp. The third beam is also used to align the detector surface parallel to it, so that it is horizontal. On top of the table above the instrument is a construction holding two mirrors. The beam used for the horizontal alignment is going through a beam splitter before it reaches the instrument. This produces an additional fourth beam, which is going vertically up to the first mirror, is then reflected over 90° to the mirror that is exactly above the center of the instrument. It then is reflected over 90° down again. At the center of the instrument there are three perpendicular laser beams: one passing through the lamp, one passing the detector surface horizontally, and one vertically. The last

beam is used for vertical alignment of the detector surface. This procedure guarantees an alignment of lamp and instrument that is reproducible as long as it is followed properly for each calibration.

Direct radiation measurements are usually performed with sensors mounted in a tube. The quartz plate that is the entrance of the tube is than used as reference plane for the alignment of the instrument. The rest of the alignment procedure is basically the same as that for the global instruments.

### 3.3.6 Wavelength calibrations

Wavelength calibrations are usually performed with spectral lamps. These are low pressure lamps containing a gas that produces spectral lines in a certain wavelength region. In the UV-calibration lab five different spectral lamps (Ar, Kr, Ne, Xe, and Hg(Ar)) are available, covering a wavelength region from 180 nm to 900 nm.

## 3.4 Summary and Concluding Remarks

Ozone and UV-monitoring are long term activities, because such measurements are intended for trend analysis. KNMI is planning to continue UV and ozone research for a long period. Therefore investments have been made in instruments to perform the measurements.

Fortunately it was also understood that UV-measurements are still in an experimental phase, and that good facilities were needed to investigate and perform calibrations at the KNMI itself. Many of the available UV-instruments do not have calibrations at all, or the calibration supplied with the instrument is incorrect (as we know by own experience). The new and unique KNMI UV-calibration laboratory provides the possibilities to perform all required types of UV-calibrations and instrument checks that are needed.

The interest of and calibrations for other research institutes and commercial companies (IMAU, Utrecht University, Kipp & Zonen) indicate that such a calibration facility was really needed in the Netherlands. The Norwegian and Finnish Meteorological Institutes also expressed their interest for calibration of their UV-instruments. National and international cooperations in this new field of research already exist, and are expected to be extended in the future.

# Chapter 4

# Spectral UV-Radiative Transfer Calculations

## 4.1 General Description of the Model Capabilities

The radiative transfer model that is used to compute ground level UV-irradiances, has also been used in NOP project no. 8520587 (Van Lammeren *et al.* 1994). Relevant information on the computational method and the model atmosphere is also briefly given here.

The Doubling-Adding radiative transfer model, called DAK (Doubling-Adding KNMI), has been developed at KNMI in the past years to simulate shortwave spectra and vertical profiles of irradiance, radiance and polarization in the Earth's atmosphere. The computer code of the DAK model consists of a monochromatic radiative transfer kernel (developed at the Free University, Amsterdam), which solves the multiple scattering problem, and a shell of atmospheric information based on actual atmospheric composition observations or climatology.

There are at least three applications of DAK

1. Simulation of radiances and polarization at the top-of-the-atmosphere (TOA) to interpret satellite measurements at solar wavelengths. Relevant satellite instruments are: GOME, SCIAMACHY, POLDER, AVHRR, Meteosat, and ATSR-2. Example of an application: retrieval of cloud optical thickness from satellite measurements of reflectivity in the visible wavelength range.

2. Simulation of spectral irradiances, radiances and polarization inside the atmosphere to interpret groundbased or airborne radiation measurements. Example of an application: interpretation of UV irradiances measured at KNMI.

3. Calculation of spectral irradiances (radiative fluxes) at TOA and inside the atmosphere to test radiation parameterizations used in climate models. Example of an application: test of a broad-band parameterization of irradiances for the UV-visible wavelength range.

The main characteristics of the DAK model are

- monochromatic; this means that a spectrum is calculated line-by-line
- the atmosphere is modelled by a stack of homogeneous, plane-parallel layers

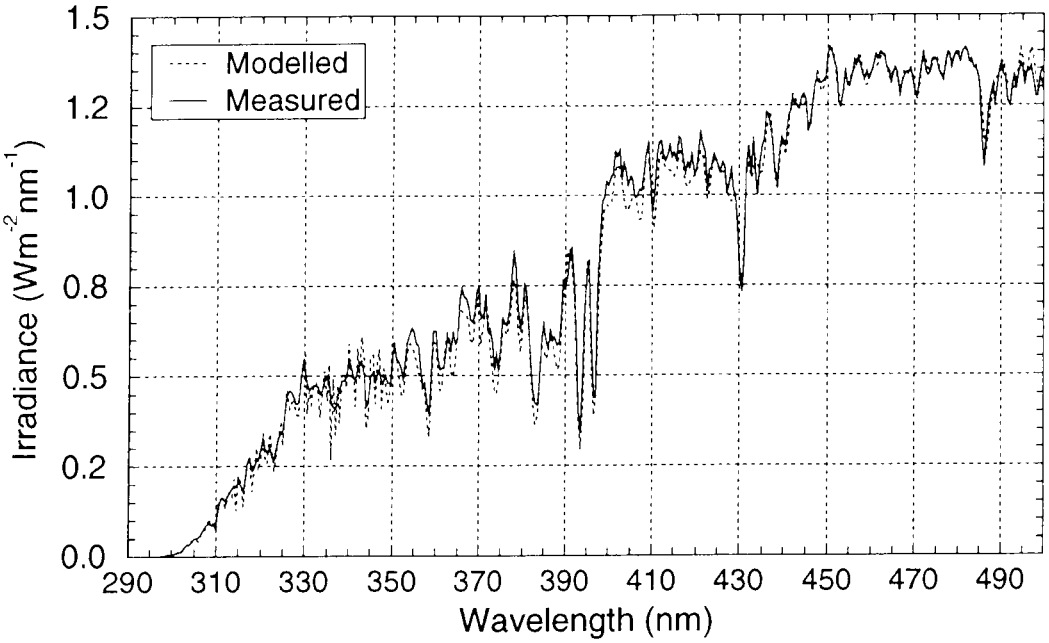


**Figure 4.1** An example of a measured (Garmisch-Partenkirchen, July 24, 1993, Austria-Innsbruck instrument) and a computed UV-spectrum.

- multiple scattering is treated exactly (as many scattering directions are taken into account as needed for a specified accuracy)
- polarization can be fully included (four Stokes parameters)
- only solar radiation is incident
- the following scattering and absorption processes are included: molecular scattering, gas absorption (only weak bands, e.g. those of $O_3$), aerosol scattering and absorption, cloud particle scattering and absorption, and surface reflection and absorption.

Compared to almost all other radiative transfer models, the DAK model is unique in its inclusion of polarization. This is important to interpret satellite measurements of polarization (which will be performed by GOME, SCIAMACHY, and POLDER), but also to accurately simulate atmospheric radiances, especially in the UV. Recently, DAK results have been successfully compared with UV irradiance measurements (Kuik *et al.* 1994), and an example of a measured and a computed UV-spectrum is shown in Fig. 4.1.

## 4.2 Details of the Model

The heart of the model is the doubling-adding algorithm. The approach of solving the problem of multiple scattering in a vertically inhomogeneous atmosphere by means of doubling and adding layers has been conceived by Van de Hulst (1980). The starting point is a very thin layer of which the reflection and transmission properties can be calculated analytically from single and double scattering. This layer is repeatedly doubled, taking into account internal reflections at the interface, until a specified optical thickness is reached and the

reflection and transmission properties of this homogeneous layer are found. By adding different layers, taking again into account the reflections at the interface, the reflection and transmission properties of a vertically inhomogeneous atmosphere can be found. The extension of the doubling-adding method to polarization has been described by De Haan *et al.* (1987) and the extension to the internal radiation field by Stammes *et al.* (1989). The doubling-adding method has been tested extensively and compared with other radiative transfer methods, and was found to be accurate and fast.

In the doubling-adding algorithm three parameters are needed for every layer of a multilayer atmosphere: *(i)* the (extinction) optical thickness, *(ii)* the single scattering albedo, and *(iii)* the scattering matrix (also called phase matrix). The latter parameter describes the angular scattering and polarization properties of a volume-element of the layer. For spherical aerosol and cloud particles a Mie program is used to calculate off-line the scattering matrix. The atmospheric shell of the program calculates these three parameters for every layer, given the following input files:

- pressure, temperature, and trace gas mixing ratio profiles, taken from radiosonde data or climatology (McClatchey *et al.* 1972)
- background aerosol concentration profile; at the moment the LOWTRAN7 aerosol climatology is included (Kneizys *et al.* 1988)
- special aerosol or cloud particle optical parameters.

At the moment shortwave spectral absorption by $O_3$, $NO_2$, and $SO_2$ is included in the model. Therefore, the model can only accurately calculate the atmospheric radiation between about 250 and 700 nm, i.e. the UV and visible range, and at specific atmospheric windows in the near-IR. A recent description of the model, with the formulae used, is given by Stammes (1994).

Various types of output from DAK are possible:

- Spectra of irradiance, radiance, and polarization at TOA or the surface for a certain wavelength range.
- Vertical profiles of irradiances and heating rate for a specific wavelength.
- Dependence of reflected and transmitted (ir)radiances of a cloud on its optical thickness.

## Chapter 5

# Concluding Remarks and Future Work

In 1991 and 1992 UV-research started at the KNMI with first tests of narrow band UV-instruments. Since then much has been achieved. At this moment instruments that will provide UV-researchers with long term measurements have been installed. Accurate ground based ozone measurements (Brewer) are performed continuously. Spectral UV-measurements (also Brewer) are recorded in between the ozone measurements, which guarantees the best possible correlation between the two types of measurements. A radiative transfer model that is able to compute spectral UV-irradiances (and several other radiative quantities), coupled to an atmosphere model, is now operational. A sophisticated UV-calibration laboratory was built at the KNMI, enabling us to perform calibrations of UV-instruments according to the highest international standards and requirements. These facilities will also be made available for other institutes to calibrate their UV-instruments.

Narrow band UV-meters are employed for monitoring purposes at a higher frequency than the spectral UV-measurements. At the moment the narrow band UV-meters are only installed at our observation site in De Bilt, but in the future other locations in the Netherlands will be equipped with these UV-instruments as well.

In January 1994 a start was made with ground based high accurate ozone monitoring employing Brewer #100. The next decades this instrument will provide an ozone climatology for The Netherlands.

Preliminary analysis of Brewer UV-data already provides some insight in the UV-climate in the Netherlands only after about ten months of measurements. From all measurements recorded up to this moment it was found that the maximum amount of DUV can be approximated by our empirical model using a total column zone of 300 DU. Spectral radiative transfer calculation of DUV for clear sky conditions show features similar to those observed in the measurements. They have proven to be useful in studying effects of solar elevation and total column ozone on ground level UV-irradiances as well.

In 1993 a discussions started with the Netherlands Cancer Association (KWF), University of Utrecht (AZU), and National Institute of Public Health and Environmental Protection (RIVM) on issuing UV-forecasts (Allaart 1994b). Brewer ozone and UV-measurements were used to validate the forecasts, and a preliminary comparison of measured and forecasted data shows good agreement. At this time the discussion is still going on with the relevant authorities on whether or not to issue such forecasts to the public. More details on the forecasting mechanism and some results are given by Allaart (1994b).

Correlation studies between cloud cover and UV-radiation showed that the highest DUV values do not occur for cloudless condition, but for several eighths of cloud cover. The narrow band UV-measurements, and also the broadband radiation meters, confirmed this phenomenon. More detailed analysis will follow, in which a number of cloud layers, cloud type, etc., will be included. Another conclusion from the normalized DUV for clear sky conditions is that a variations of approximately 20% remains if only ozone and solar elevation are taken into account. This 20% variation is caused by aerosol, ground albedo, and may be some unknown parameters. Especially effects of aerosol will be investigated in detail in the future.

Monitoring data has become available only since January 1994. A start has been made with the analysis of this data, but it has by no means finished yet. In the near future more and other correlation studies will be undertaken using cloud cover data. The results may be improved by trying to couple measurements of global, direct, and diffuse radiation to obtain an observer-independent quantity for cloud cover.

Several instrument intercomparison campaigns, national and international, have provided valuable information on instrument performances. These useful campaigns will be continued the coming year(s), and international cooperation with other meteorological institutes on UV and ozone research will be extended and intensified.

# References

Allaart, M.A.F., Kelder, H., and Heijboer, L.C., "On the Relation Between Ozone and Potential Vorticity", Geophys. Res. Lett. **20**, 811–814 (1993).

Allaart, M.A.F., Private Communication (1994a).

Allaart, M.A.F., and Kelder, H., "Meteorological aspects of global modelling of atmospheric chemistry (GLOMAC)", Final Rep. NOP project no. 851050 (1994b).

Bais, A.F., Zerefos, C.S., Meleti, C., Ziomas, I.C., and Tourpali, K., "Spectral Measurements of Solar UVB Radiation and its Relation to Total Ozone, $SO_2$, and Clouds", J. Geophys. Res. **98**, 5199–5204 (1993).

Blumthaler, M., and Ambach, W., "Indication of Increasing Solar Ultraviolet-B Radiation Flux in Alpine Regions", Science **248**, 206–208 (1990).

Brasseur, G., "Volcanic Aerosol Implicated", Nature **359**, 275–276 (1992).

Brühl, C., and Crutzen, P.J., "On the Disproportionate Role of Tropospheric Ozone as a Filter against Solar UV-B Radiation", Geophys. Res. Lett. **16**, 703–706 (1989).

Caldwell, M.M., Camp, L.B., Warner, C.W., and Flint, S.D., "Action Spectra and Their Key Role in Assessing the Biological Consequences of Solar UV-B Radiation Change", in R.C. Womest and M.M. Caldwell (eds.), *Stratospheric Ozone Reduction, Solar Ultraviolet Radiation and Plant Life*, Springer-Verlag, pp. 87–111 (1986).

Chapman, S., "A Theory of Upper Atmospheric Ozone", R. Meteorol. Soc. Mem. **3**, 103–125 (1930).

Dahlback, A., Henriksen, T., Larsen, S.H., and Stamnes, K., "Biological UV-Doses and the Effect of an Ozone Layer Depletion", Photochemistry and Photobiology **49**, 621–625 (1989).

De Haan, J.F., Bosma, P.B., and Hovenier, J.W., "The Adding Method for Multiple Scattering Calculations of Polarized Light", Astron. Astrophys. **183**, 371–391 (1987).

Frederick, J.F., Snell, H.E., and Haywood, E.K., "Solar Ultraviolet Radiation at the Earth's Surface", Photochemistry and Photobiology **50**, 443–450 (1989).

Frederick, J.F., and Snell, H.E., "Tropospheric Influence on Solar Ultraviolet Radiation: The Role of Clouds", J. Climate **3**, 373–381 (1990).

Gardiner, B.G., and Kirsch, P.J. (eds.), *Second European Intercomparison of Ultraviolet Spectroradiometers, 21–31 August 1992*, Panorama, Greece (1993).

Gardiner, B.G., and Kirsch, P.J. (eds.), *Setting Standards for European Ultraviolet Spectroradiameters*, Report to the Commision of the European Communities, Step Project 76 (1994).

*Guide to Meteorological Instruments and Methods of Observations*, 5th ed., WMO No. 8, Secr. of the WMO, Geneva (1983).

Kerr, J.B., McElroy, C.T., and Wardle, D.I., "The Automated Brewer Spectrophotometer", Proc. Quadr. Ozone Symp. Halkidiki 1984, Zerefos, C.S., and Ghazi, A (eds.), D. Reidel, Norwell, Mass. 396–401 (1985).

Kerr, J.B., McElroy, C.T., and Olafson, R.A., "Measurements of Ozone with the Brewer Ozone Spectrophotometer" Proc. Quadr. Ozone Symp. **1**, Boulder, Col. (1990).

Kerr, J.B., McElroy, C.T., Tarasick, D., and Wardle, D.I., "The Canadian Ozone Watch and UV-B Advisory Programs", in *Ozone in the Troposphere and Stratosphere, Part 2*, Proc. Quadr. Ozone Symp. Charlottesville 1992, NASA CP-3266, 794–799 (1994).

Kerr, J.B., and McElroy, C.T., "Evidence of Large Upwards Trends of Ultraviolet-B Radiation Linked to Ozone Depletion", Science **262**, 1032–1034 (1994).

Kerr, R.A., "Ozone takes a Nose Dive after the Eruption of Mt. Pinatubo", Science **260**, 490–491 (1993).

Kipp & Zonen, Private Communication (1994).

KMI, RIVM, and KNMI, *Recente Ontwikkelingen in de Ozonlaag en de Ultraviolette Straling boven Nederland* (1993).

Kneizys F.X., Shettle, E.P., Abrue, L.W., Chetwynd, J.H., Anderson, G.P., Gallery W.O., Selby, J.E.A., and Clough, S.A., *Users Guide to LOWTRAN 7*, AFGL-TR-88-0177, Environmental Research Papers No. 1010, Hanscom AFB, Mass. (1988).

Kuik, F., Wauben, W.M.F., and Stammes, P., "Modelling the Influence of Aerosol on the Observed UV Spectrum", in *Abstracts: Conference on Aerosols and Atmospheric Optics*, Malm, W.C., and Mueller, P.K. (eds.)Snowbird, Utah, USA, Sept. 25–30 (1994).

Lubin, D., and Frederick, J.F., "The Ultraviolet Radiation Environment of the Antartic Peninsula: The Roles of Ozone and Cloud Cover", J. Appl. Meteor. **30**, 478–493 (1991).

McClatchey, R.A., Fenn, R.W., Selby, J.E.A., Volz, F.E., and Garing, J.S., *Optical Properties of the Atmosphere*, 3-rd ed., AFCRL-72-0497, Environmental Research Papers No. 411, Air Force Cambridge Research Labs., Bedford, Mass. (1972).

McKenzie, R.L., Matthews, W.A., and Jonston, P.V., "The Relationship Between Erythemal UV and Ozone Derived from Spectral Irradiance Measurements", Geophys. Res. Lett. **18**, 2269–2272 (1991).

McKinlay, A.F., and Diffey, B.L., "A Reference Action Spectrum for Ultra-Violet Induced Erythema in Human Skin", in W.F. Passchier and B.F.M. Bosnajakovic (eds.), *Human Exposure to Ultraviolet Radiation: Risks and Regulations*, Elsevier, pp. 83–87 (1987).

Mimms III, F.M., and Frederick, J.E., "Cumulus Clouds and UV-B", Nature **371**, 291 (1994).

Scotto, J., Cotton, G., Urbach, F. Berger, D., and Fears, T., "Biologically Effective Ultraviolet

Radiation: Surface Measurements in the United States, 1974 to 1988", Science **239**, 762–764 (1988).

Setlow, R.B., "The Wavelengths in Sunlight Effective in Producing Skin Cancer: A Theoretical Analysis", Proc. Nat. Acad. Sci. USA **71**, 3363–3366 (1974).

Spinhirne, J.D., and Green, A.E.S., "Calculations of the Relative Influence of Cloud Layers on the Received Ultraviolet and Integrated Solar Radiation", Atmos. Environ. **12**, 2449–2454 (1978).

Stammes, P., de Haan, J.F., and Hovenier, J.W., "The Polarized Internal Radiation Field of a Planetary Atmosphere", Astron. Astrophys. **225**, 239–259 (1989).

Stammes, P., "Errors in UV Reflectivity and Albedo Calculations due to Neglecting Polarisation", Proceedings of the European Symposium on Satellite Remote Sensing, 26–30 Sept. 1994, Rome, EOS/SPIE **2311** (1994).

Stamnes, K., Slusser, J., Bowen, M., Booth, C., and Lucas, T., "Ultraviolet Radiation, Total Ozone Abundance, and Cloud Optical Depth at McMurdo Station, Antartica September 15 1988 through April 15 1989", Geophys. Res. Lett. **17**, 2181–2184 (1990).

Stamnes, K., "The Stratosphere as a Modulator of Ultraviolet Radiation into the Biosphere", Surv. Geophys. **14**, 167–186 (1993).

Tsay, S-C., and Stamnes, K., "Ultraviolet Radiation in the Artic: The Impact of Potential Ozone Depletion and Cloud Effects", J. Geophys. Res. **97**, 7829–7840 (1992).

Van de Hulst, H.C., *Multiple Light Scattering, Tables, Formulas, and Applications; Volume 1 and 2*, Academic Press, New York (1980) .

Van der Leun, J. (chair.), Health Counsil Commision 'Risico's UV straling', *UV Straling uit Zonlicht*, Den Hague (1994).

Vanhoosier, M.E., Bartoe, J-D.F., Brueckner, G.E., and Prinz, D.K., "Absolute Solar Spectral Irradiance 120 nm – 400 nm (Results from the Solar Ultraviolet Spectral Irradiance Monitor -SUSIM- Experiment on Board Spacelab 2)", Astro. Lett. and Communications **28**, 163–168 (1988).

Van Lammeren, A.C.A.P., Feijt, A.J., Van Dorland, R., Van Meijgaard, E., and Stammes, P., "Clouds–Radiation–Hydrologic interactions in a limited-area model", Final Rep. NOP project no. 8520587 (1994).

Watson, R.T., Prather, M.J., and Kurylo, M.J., *Present State of Knowledge of the Upper Atmosphere: An Assessment Report*, NASA Reference Publication 1208, Washington DC (1988).

Wayne, R.P., *Chemistry of Atmospheres*, 2nd ed., Oxford Univ. Press, Oxford (1991).

Whitten, R.C., and Prasad, S.S. (eds.), *Ozone in the Free Atmosphere*, Van Nostrand Reinhold, New York (1985).

Wilson, L., Vallée, M., Tarasick, D., Kerr, J.B., and Wardle, D., "Operational Forecasting of Daily Total Ozone and Ultraviolet-B Radiation Levels for Canada", Research Report No. (MSRB/ARQX) 92–004 (1992).

WMO/UNEP, *Scientific Assessment of Ozone Depletion: 1994.*

Bijgaand treft U een overzicht aan van recentelijk in deze serie gepubliceerde titels. Een komplete lijst wordt U op verzoek toegezonden. U kunt Uw aanvraag richten aan de KNMI Bibliotheek, Postbus 201, 3730 AE De Bilt (030-206855). Hier kan men U tevens informeren over de verkrijgbaarheid en prijzen van deze publicaties.

89-01 Instability mechanisms in a barotropic atmosphere / R.J. Haarsma.

89-02 Climatological data for the North Sea based on observations by voluntary observing ships over the period 1961-1980 / C.G. Korevaar.

89-03 Verificatie van GONO golfverwachtingen en van Engelse fine-mesh winden over de periode oktober 1986 - april 1987 / R.A. van Moerkerken.

89-04 Diagnostics derivation of boundary layer parameters from the outputs of atmospheric models / A.A.M. Holtslag and R.M. van Westrhenen.

89-05 Statistical forecasts of sunshine duration / Li Zhihong and S. Kruizinga.

90-01 The effect of a doubling atmospheric CO2 on the stormtracks in the climate of a general circulation model / P.C. Siegmund.

90-02 Analysis of regional differences of forecasts with the multi-layer AMT-model in the Netherlands / E.I.F. de Bruin, Li Tao Guang and Gao Kang.

90-03 Description of the CRAU data-set : Meteosat data, radiosonde data, sea surface temperatures : comparison of Meteosat and Heimann data / S.H. Muller, H. The, W. Kohsiek and W.A.A. Monna.

90-04 A guide to the NEDWAM wave model / G. Burgers.

91-01 A parametrization of the convective atmospheric boundary layer and its application into a global climate model / A.A.M. Holtslag, B.A. Boville and C.-H. Moeng.

91-02 Turbulent exchange coefficients over a Douglas fir forest / F.C. Bosveld.

92-01 Experimental evaluation of an arrival time difference lightning positioning system / H.R.A.Wessels.

92-02 GCM control run of UK Meteorological Office compared with the real climate in the NW European winter / J.J. Beersma.

92-03 The parameterization of vertical turbulent mixing processes in a General Circulation Model of the Tropical Pacific / G. Janssen.

92-04 A scintillation experiment over a forest / W.Kohsiek.

92-05 Grondtemperaturen / P.C.T.van der Hoeven en W.N.Lablans

92-06 Automatic supression of anomalous propagation clutter for noncoherent weather radars / H.R.A. Wessels and J.H. Beekhuis.

93-01 Searching for stationary stable solutions of Euler's equation / R. Salden.

93-02 Modelling daily precipitation as a function of temperature for climatic change impact studies / A.M.G. Klein Tank and T.A. Buishand.

93-03 An analytic conceptual model of extratropical cyclones / L.C. Heijboer.

93-04 A synoptic climatology of convective weather in the Netherlands / Dong Hongnian.

93-05 Conceptual models of severe convective weather in the Netherlands / Dong Hongnian.

94-01 Seismische analyse van aardbevingen in Noord-Nederland : bijdrage aan het multidisciplinaire onderzoek naar de relatie tussen gaswinning en aardbevingen / H.W.Haak en T. de Crook.

94-02 Storm activity over the North Sea and the Netherlands in two climate models compared with observations / J.J. Beersema.

94-03 Atmospheric effects of high-flying subsonic aircraft / W. Fransen.

94-04 Cloud-radiation-hydrological interactions : measuring and modeling / A.J. Feijt, R. van Dorland, A.C.A.P. van Lammeren, E. van Meijgaard en P. Stammes.